Solvent-free infrared polymerization of lactic acid: toward greener PLA production

Maria Montrone,[1] Cosimo Cardellicchio,[2] Jennifer Gubitosa[1], Paola Fini,[3], Mattia Di Maro[4], Donatella Duraccio[4], Paola Amazio[5] ,Pietro Cotugno,[1] Gianluca M. Farinola,[1] Maria Annunziata M. Capozzi[1*]

[1]Department of Chemistry, University of Bari "Aldo Moro", Via Orabona 4, Bari, 70125, Italy.

[2]CNR-ICCOM, Istituto di chimica dei composti organometallici, Via Orabona 4, Bari, 70125, Italy.

[3] Institute for Chemical-Physical Processes - IPCF of Bari, Italian National Council of Research – CNR, Via Orabona, 4, 70125, Bari, Italy.

[4] Institute of Sciences and Technologies for Sustainable Energy and Mobility, National Council of Research, Strada delle cacce 73, 10135 Torino, Italy.

[5] NEXT TECHNOLOGY TECNOTESSILE, Società Nazionale di Ricerca R.L., via del Gelso 13 Prato, Italy.

*Corresponding author. e-mail: maria.capozzi@uniba.it

Contributing authors: maria.montrone@uniba.it; cardellicchio@ba.iccom.cnr.it; jennifer.gubitosa@uniba.it; p.fini@ba.ipcf.cnr.it; nextsud@tecnotex.it; mattia.dimaro@stems.cnr.it; donatella.duraccio@stems.cnr.it; pietro.cotugno@uniba.it; gianlucamaria.farinola@uniba.it; maria.capozzi@uniba.it.

Contents

S1. General Remarks

S1.1 Reagents and Instrumentation

DL-Lactic Acid (85% in water) (CAS RN50-21-5) and L-lactic acid (85% in water) (CAS RN79-33-4) were purchased from TCI Europe (Paris, France) and were used as received. Indium(III)trifluoromethanesulfonate,Ytterbium(III)trifluoromethanesulfonate(99.99%), Zinc trifluoromethanesulfonate (98%), Scandium(III)trifluoro-methanesulfonate (99%), p-Toluenesulfonic acid monohydrate (98.5%), Terbium(III) chloride hexahydrate (99.9% trace metals basis), Ytterbium(III) chloride hexahydrate (99.9% trace metals basis), ZnO (ReagentPlus®, powder, <5 μm particle size, 99.9%), MoO_3 (ACS reagent, ≥99.5%), Montmorillonite K 10, were purchased from Merck. Bismuth(III)trifluoromethanesulfonate (99.2%), Indium(III) chloride (99.99%) were purchased from BDLpharm. Zirconium(IV) chloride (99.5% Zr) was purchased from "abcr". Dichloromethane (DCM), methanol (MeOH) were purchased from Merck and were used for the purifications . Preparative column chromatography was carried out using Macherey–Nagel silica gel (Macherey–Nagel, Düren, Germany) (60, particle size 0.063–0.2 mm).

Reactions under IR irradiation were carried out using a Philips Infrared IndustrialHeat Br125 IR 250 W 230–250 VCL 1CT incandescent lamp.

^{1}H-NMR, ^{13}C-NMR spectra were recorded on an Agilent 500 spectrometer (Agilent Technologies, Santa Clara, CA, USA) at 500 and at 125 MHz, respectively. $CDCl_3$ was used as the deuterated solvent.

FT-IR spectra were measured on a spectrophotometer Bruker Invenio-S FT-IR (Bruker, Billerica, MA, USA) using dry KBr pellets with the scan range 4000–400 cm^{-1}.

Polarimetric measurements of the samples were performed on a Perkin Elmer Model 343 Polarimeter (589 nm): the angle of the optical rotation of polymers was determined in a CH_2Cl_2 solution at 25 °C.

Thermal stability, decomposition temperature, and char yield of racemic PLA and PLLA were investigated by a **Thermogravimetric Analyzer** (TGA-Perkin Elmer Pyris 1). The glass transition temperature and the melting/crystallization behaviour of samples were evaluated by **differential scanning calorimetric** measurements using a DSC-Q200 – TA Instruments.

Gel permeation chromatography (GPC) was performed on an VISCOTEK TDA 305 HPLC system equipped with TOSOH Corporation (Tokyo, Japan), columns (TSKgel G3000HHR, column size 7.8 mm I.D. × 30 cm, particle size 5 μm) and IR detector. A mixture of THF/$CHCl_3$ 9:1 was used as the mobile phase at a flow rate of 1.0 mL min−1. Polystyrene standards were used for establishing the calibration curve. The PLA polymers (~5 mg) were dissolved in tetrahydrofuran/$CHCl_3$ 9:1 (5 mL). Bath sonication was employed to assist the dispersion and solution of each polymer, and the solutions were filtered through a 0.45 μm membrane filter before GPC analysis.

The number-averaged molecular weight (Mn), weight-averaged molecular weight (Mw), and polydispersity index (PDI) were calculated relative to linear PS standard.

S2. Apparatus and Setup Reaction

Figure S1: Apparatus reaction.

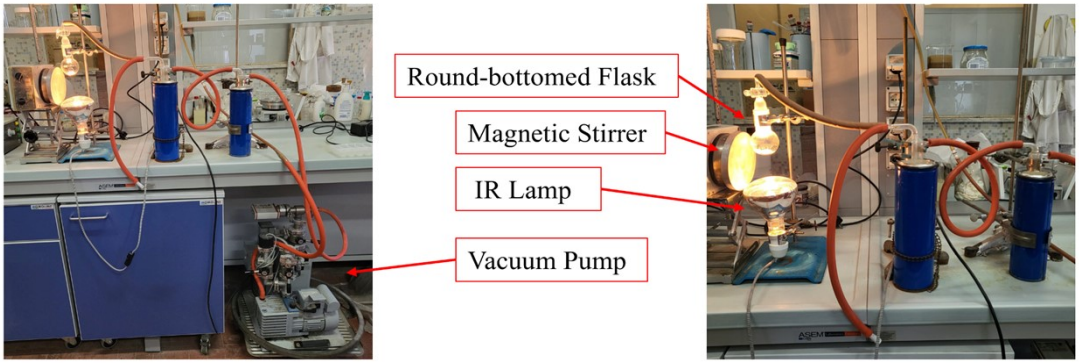

Figure S2: Apparatus for under vacuum reaction.

Figure S3: Apparatus for conventional heating reaction.

Figure S4: Apparatus for scale-up reaction.

S3. Synthetic procedure for IR-assisted Polycondensation

S3.1 Metal Triflates: General procedure

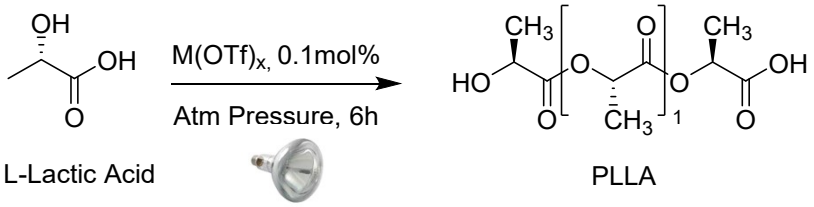

L-lactic acid (2 g, $2.2*10^{-2}$ mol) and the first rate of catalyst (0.05%mol respect of lactic acid, $1.1*10^{-5}$ mol) were added to a small crucible glass equipped with a magnetic stirrer under IR lamp (the lamp is held from the bottom of the crucible for 2h at a distance of 13 cm, for 30 min at 11.5 cm and finally at 9 cm) as shown in Figure S1. After one hour and thirty minutes, a second rate of catalyst (0.05%mol respect of lactic acid,

$1.1*10^{-5}$ mol) was added and the reaction continued for four hours and half. After about six hours of polymerization, dichloromethane was added to dissolve the polymer. The reaction solution was percolated over 3 cm of SiO_2 to remove the catalyst and the unreacted reagent. The solvent was evaporated under reduced pressure. Products were characterized by ^1H NMR and GPC.

Entry 1, Table S1 and Entry 4, Table S1 were subjected to further polymerization at 150°C for 3 hours and 30 minutes with 0.1%mol of catalyst on the heating plate, as shown in Figure S3. Subsequently, they were dissolved in DCM *q.s.* and precipitated in cold methanol. After centrifugation (20 minutes, 3000 rpm), polymers perfectly purified have been obtained (Entry 6 and 7, Table S1). They were also characterized by ^{13}C NMR, HSQC and FTIR.

Table S1: Screening Metal Triflates

Entry	$M(OTf)_x$	Yield %	Melting point (°C)	Aspect
1	**$Sc(OTf)_3$**	63	142-144	White powder
2	**$Zn(OTf)_2$**	33	98-100	White powder
3	**$Yb(OTf)_3$**	64	106-108	White powder
4	**$Bi(OTf)_3$**	67	136-138	White powder
5	**$In(OTf)_3$**	66	138-140	White powder
6	**$Sc(OTf)_3$**	47	155-157	White powder
7	**$Bi(OTf)_3$**	32	148-150	White powder

S3.2 Metal Chlorides: General Procedure

Procedure 1: without dehydration

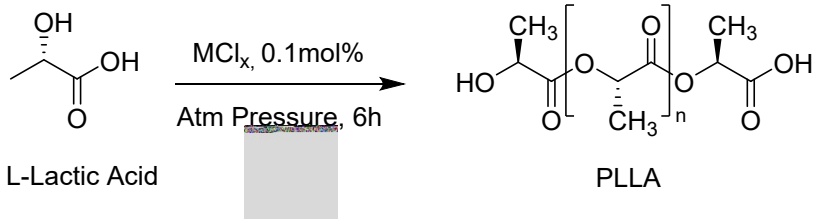

L-lactic acid (2 g, $2.2*10^{-2}$ mol) and the first rate of catalyst (0.05%mol respect of lactic acid, $1.1*10^{-5}$ mol) were added to a small crucible glass equipped with a magnetic stirrer under IR lamp (the lamp is held from the bottom of the crucible for 2h at a distance of 13 cm, for 30 min at 11.5 cm and finally at 9 cm), as shown in Figure S1. After one hour and thirty minutes, a second rate of catalyst (0.05%mol respect of lactic acid, $1.1*10^{-5}$ mol) was added and the reaction continued for four hours and half. After about six hours of polymerization, dichloromethane was added to dissolve the polymer. The reaction solution was percolated over 3 cm of SiO_2 to remove the catalyst and the unreacted reagent. The solvent was evaporated under reduced pressure. Products were characterized by ^1H NMR and GPC.

Table S2: Screening Metal Chlorides

Entry	MCl_x	Yield %	Aspect
1	**$TbCl_3*6H_2O$**	39	Transparent Gel
2	**$YbCl_3*6H_2O$**	37	Transparent Gel
3	**$InCl_3$**	34	Transparent Gel

4	**$ZnCl_2$**	50	Waxy white solid
5	**$FeCl_3$**	31	Orange Gel
6	**$ZrCl_4$**	38	Transparent Gel

Procedure 2: with dehydration

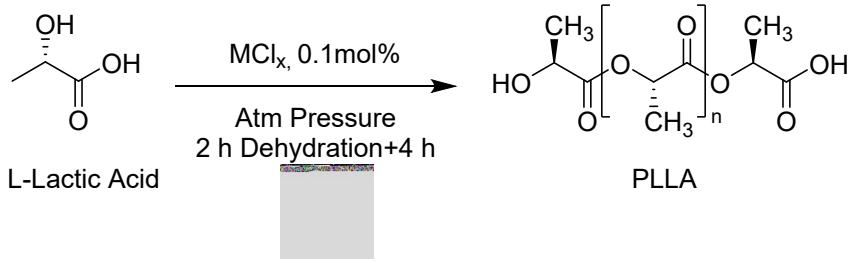

L-lactic acid (2 g, $2.2*10^{-2}$ mol) was added to a small crucible glass equipped with a magnetic stirrer under IR lamp (the lamp is held from the bottom of the crucible for 2h at a distance of 13 cm, for 30 min at 11.5 cm and finally at 9 cm), as shown in Figure S1. After two hours of dehydration, catalyst (0.1%mol respect of lactic acid, $2.2*10^{-5}$) was added and the reaction continued for four hours. After six hours of polymerization, dichloromethane was added to dissolve the polymer. The reaction solution was percolated over 3 cm of SiO_2 to remove the catalyst and the unreacted reagent. The solvent was evaporated under reduced pressure. Products were characterized by ^{1}H NMR and GPC.

Table S3: Screening Metal Chlorides

Entry	MCl_x	Yield %	Aspect
1	**$InCl_3$**	33	Transparent Gel
2	**$ZrCl_4$**	43	Transparent Gel

S3.3 Metal Oxides: General Procedure

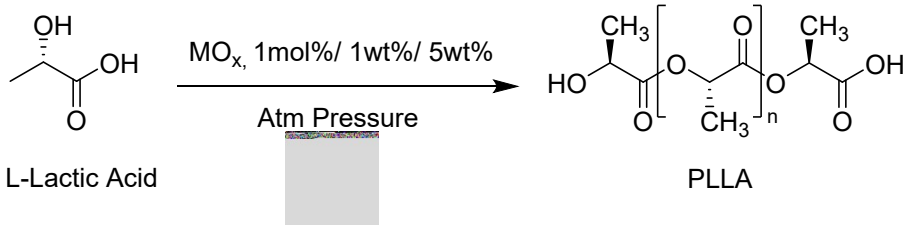

L-lactic acid (2 g, $2.2*10^{-2}$ mol) and catalyst (TiO_2: 1%mol respect of lactic acid, $2.2*10^{-4}$ mol; ZnO: 5%w respect of lactic acid, 0.1 g; Montmorillonite K10, SiO_2, MoO_3: 1%w respect of lactic acid, 0.02 g) were added to a small crucible glass equipped with a magnetic stirrer under IR lamp (the lamp is held from the bottom of the crucible for 2h at a distance of 13 cm, for 30 min at 11.5 cm and finally at 9 cm), as shown in Figure S1. Polymerization was stopped when water evaporation ended (TiO_2: 5 h e 30'; ZnO: 5 h; Montmorillonite K10: 6 h; SiO_2: 7 h; MoO_3: 10 h). Then, dichloromethane was added to dissolve the polymer. The reaction solution was percolated over 3 cm of SiO_2 to remove the catalyst and the unreacted reagent. The solvent was evaporated under reduced pressure. Products were characterized by ^{1}H NMR and GPC.

Table S4: Screening Metal Oxides

Entry	MO_x	Yield %	Aspect
1	**TiO_2**	28	Transparent Gel
2	**ZnO**	N.d.	White Solid
3	**Montmorillonite K10**	46	Transparent Gel
4	**SiO_2**	38	Transparent Gel
5	**MoO_3**	30	Transparent Gel

S3.4 Organic Protic Acids: General Procedure

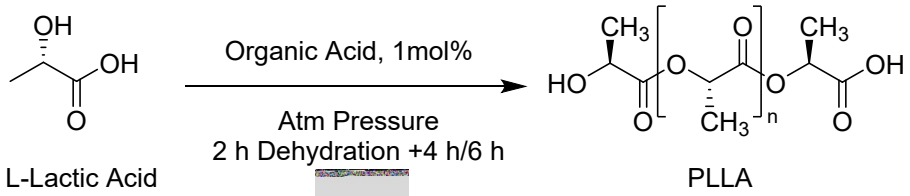

L-lactic acid (2 g, $2.2*10^{-2}$ mol) was added to a small crucible glass equipped with a magnetic stirrer under IR lamp (the lamp is held from the bottom of the crucible for 2h at a distance of 13 cm, for 30 min at 11.5 cm and finally at 9 cm), as shown in Figure S1. After two hours of dehydration, catalyst (1%mol respect of lactic acid, $2.2*10^{-4}$) was added and the reaction continued for four hours. After six hours of polymerization, dichloromethane was added to dissolve the polymer. The reaction solution was percolated over 3 cm of SiO_2 to remove the catalyst and the unreacted reagent. The solvent was evaporated under reduced pressure. Products were characterized by ^{1}H NMR and GPC.

NMR spectrum of PLLA entry 1, table 6

^{1}H-NMR (500 MHz; $CDCl_3$): δ 5.17 (q, J=7.1 Hz, 1H), 4.35 (q, J = 6.9 Hz, 1H), 1.58 (d, J = 7.1 Hz, 3H), 1,50 (d, J = 6.9 Hz, 3H).

^{13}C-NMR (125 MHz; CDCl3): δ 169.7, 69.0, 66.7, 16.7.

Table S5: Screening Protic Organic Acid

Entry	Organic Acid	Yield %	Aspect

1	**p-TSA**	80	White Solid
2	**Croconic Acid**	47	Transparent Gel
3	**Citric Acid**	47	Transparent Gel
4	**Amberlist A27**	60	Transparent Gel

S4. ^{1}H NMR/^{13}C NMR/HSQC spectra

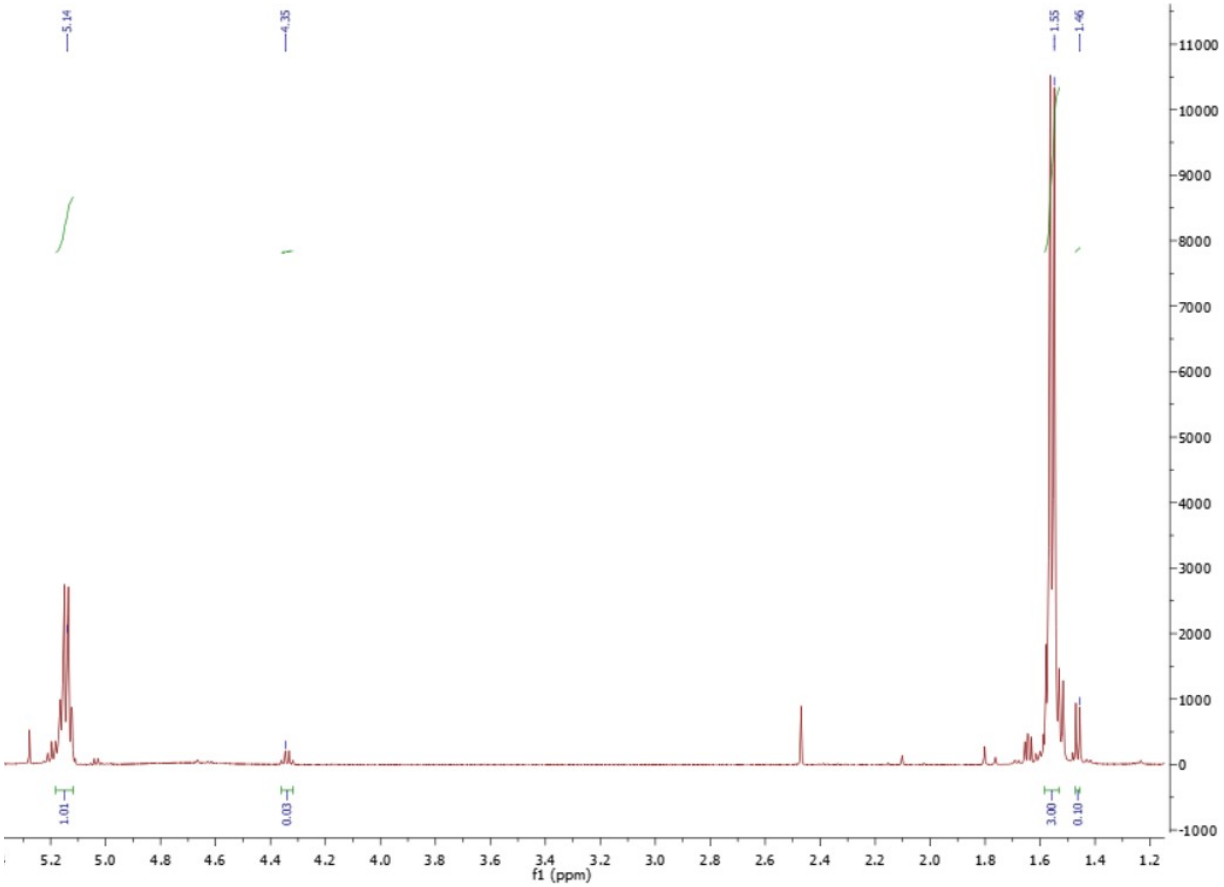

Figure S5: ^{1}H-NMR (500 MHz, $CDCl_3$) spectrum of Entry 2 (Table 3).

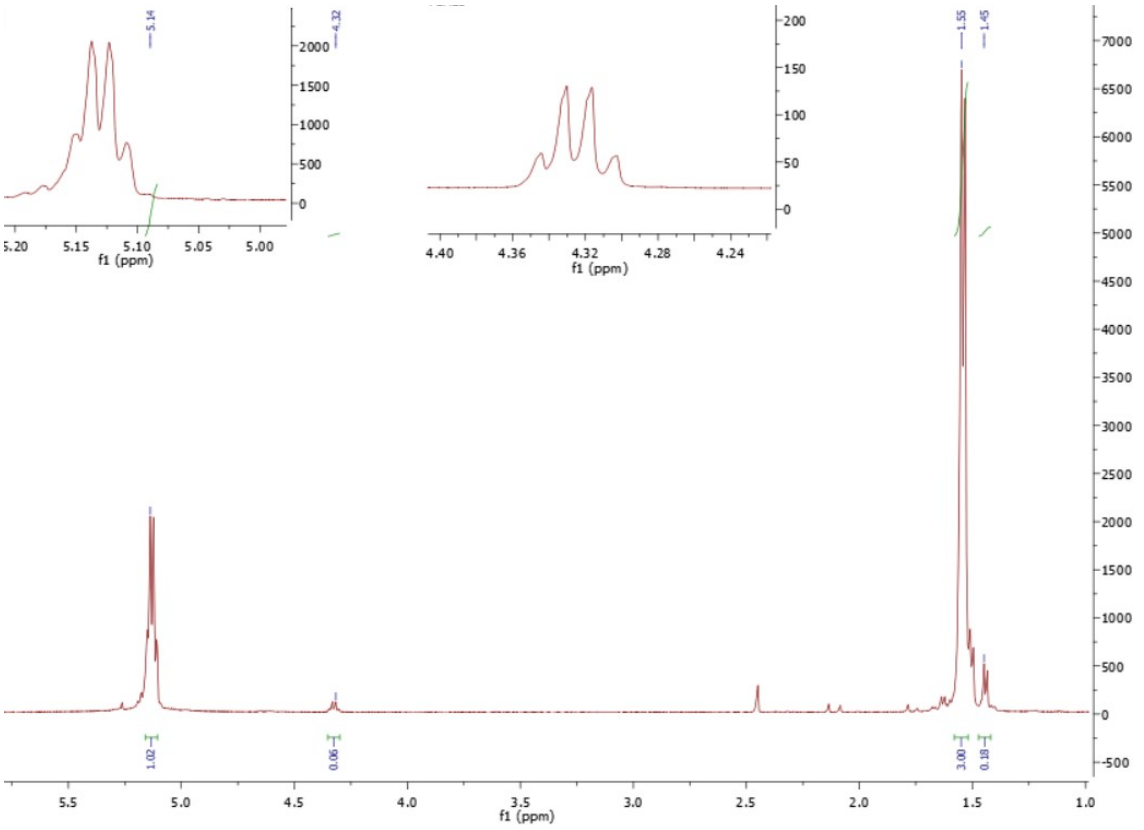

Figure S6: ^{1}H-NMR (500 MHz, $CDCl_3$) spectrum of Entry 3 (Table 3).

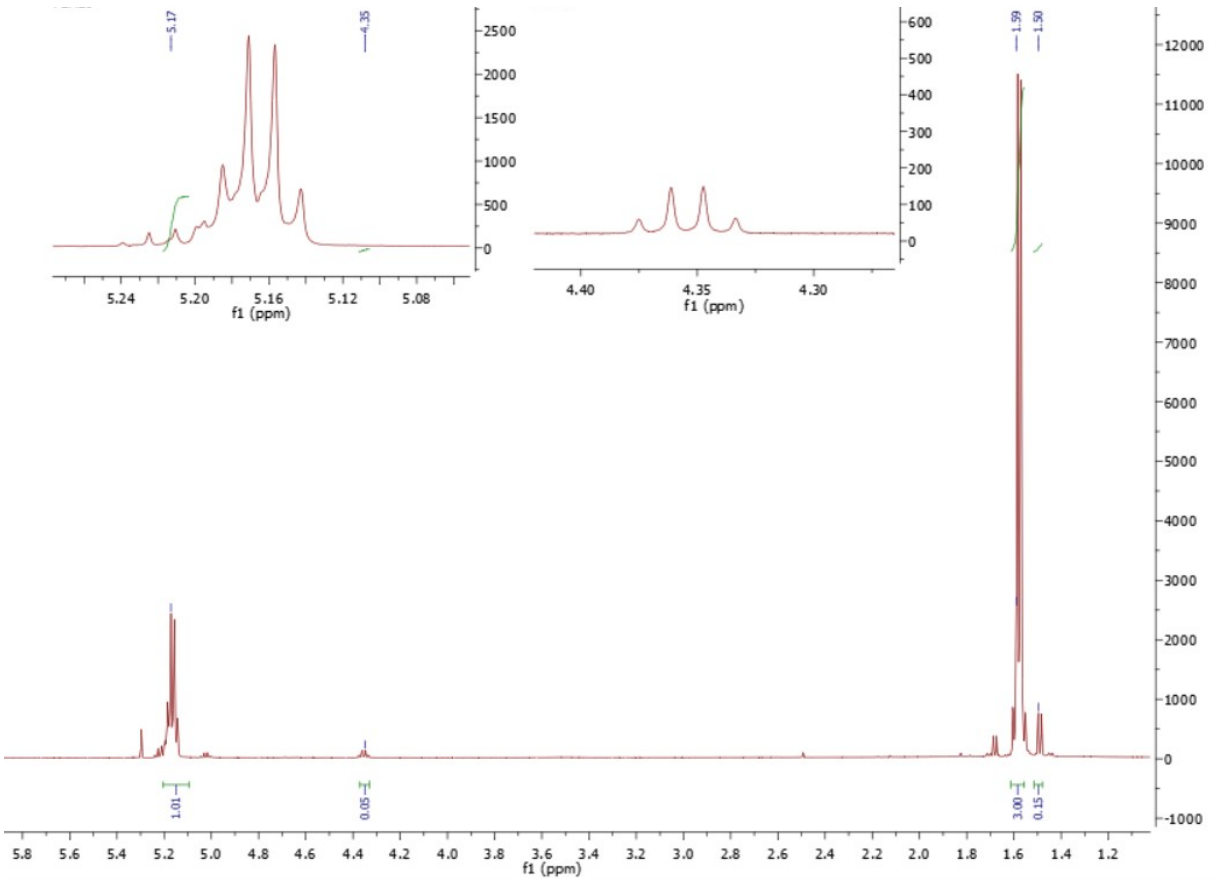

Figure S7: ^{1}H NMR(500 MHz, $CDCl_3$) spectrum of Entry 4 (Table 3).

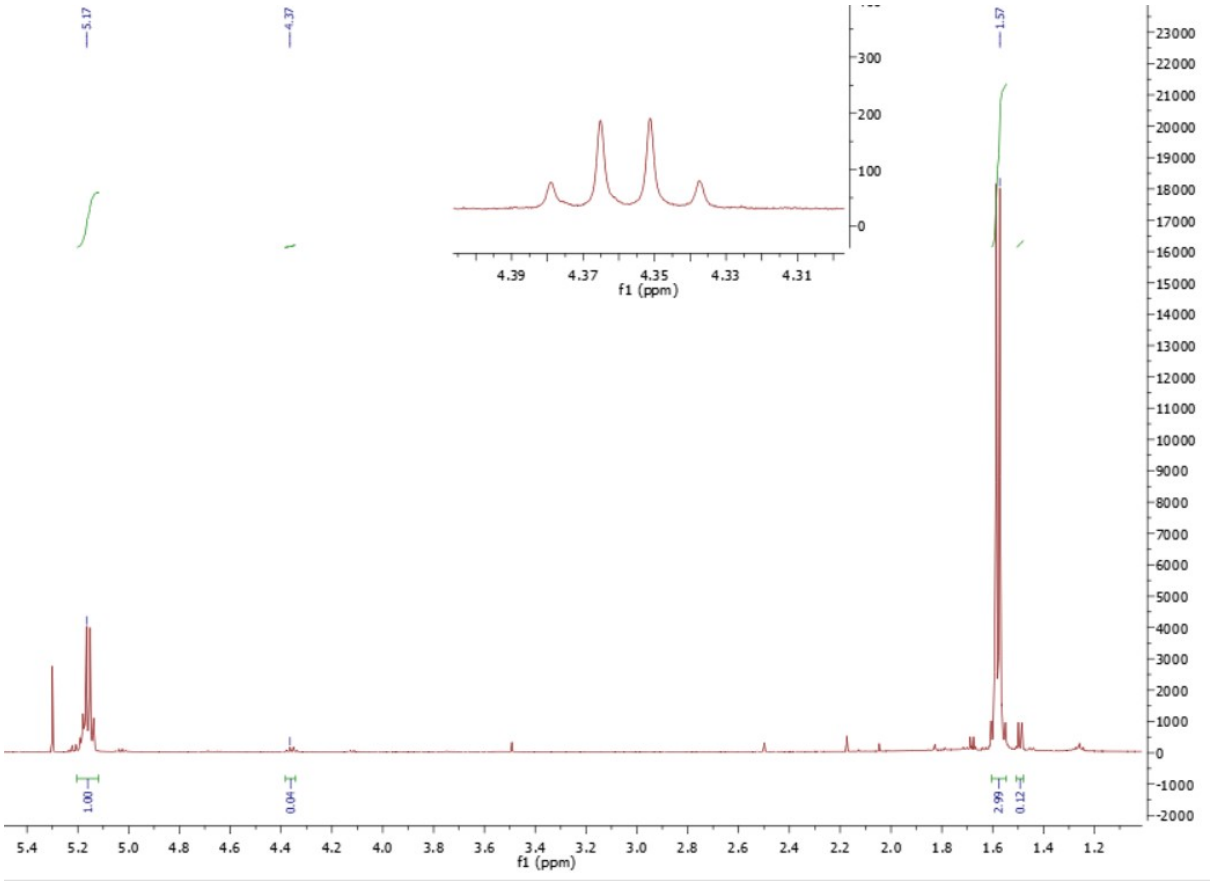

Figure S8: ^{1}H NMR (500 MHz, $CDCl_3$) spectrum of Entry 5 (Table 3).

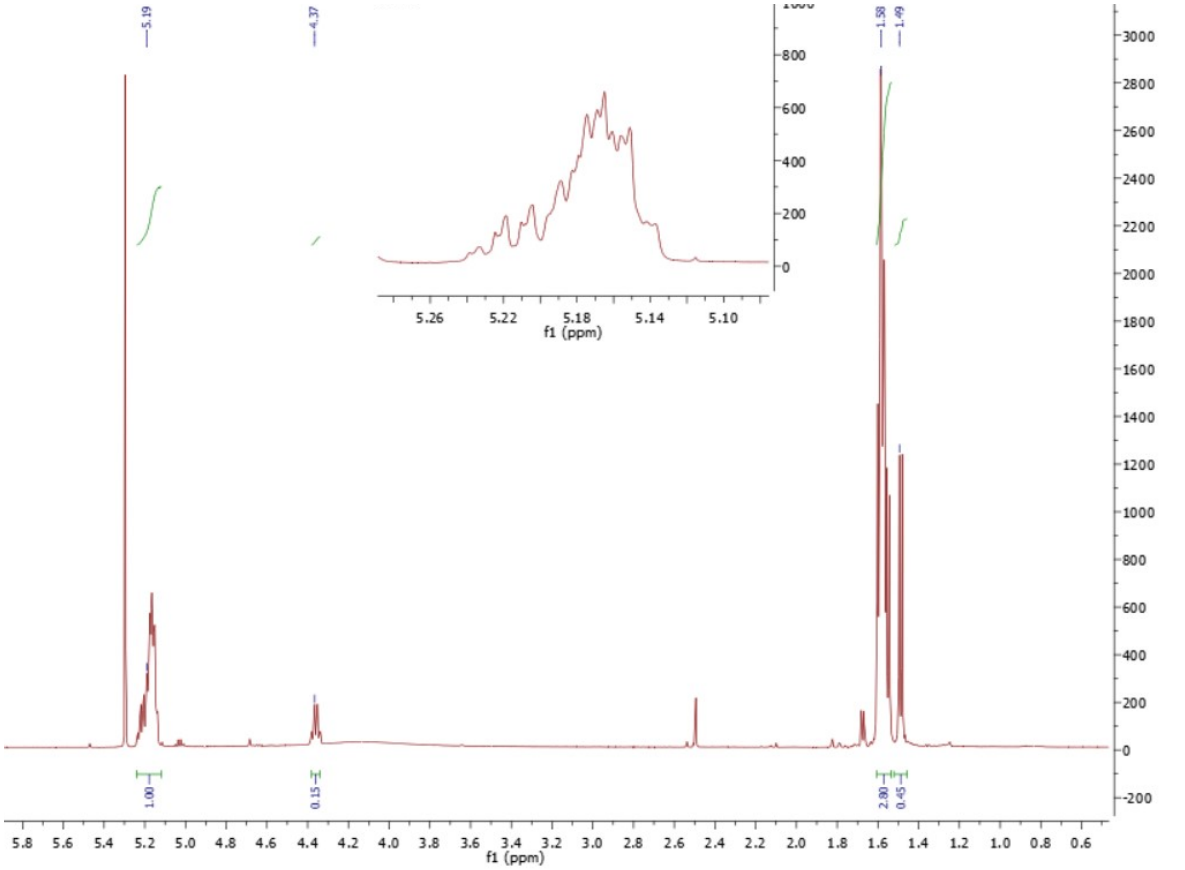

Figure S9: ^{1}H NMR (500 MHz, $CDCl_3$) spectrum of Entry 1 (Table 4).

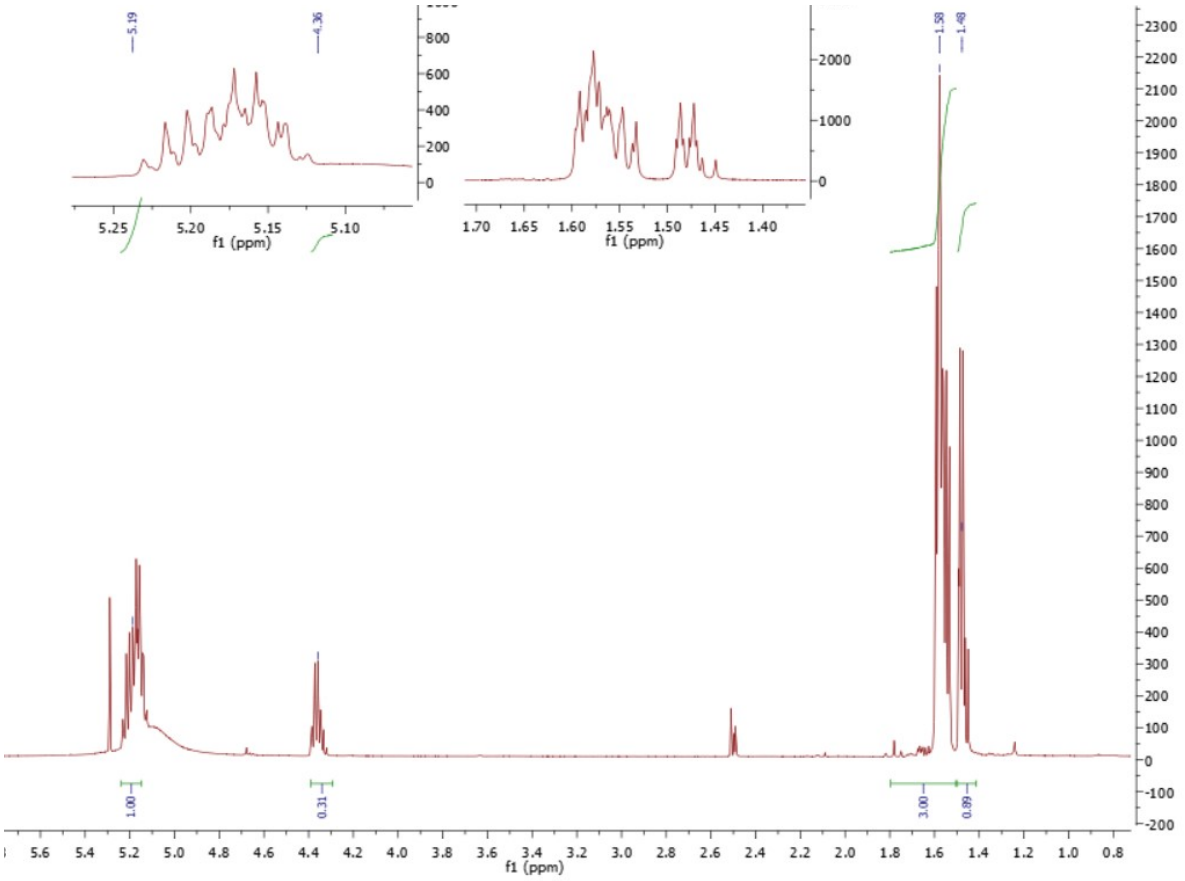

Figure S10: ^{1}H NMR (500 MHz, $CDCl_3$) spectrum of Entry 2 (Table 4).

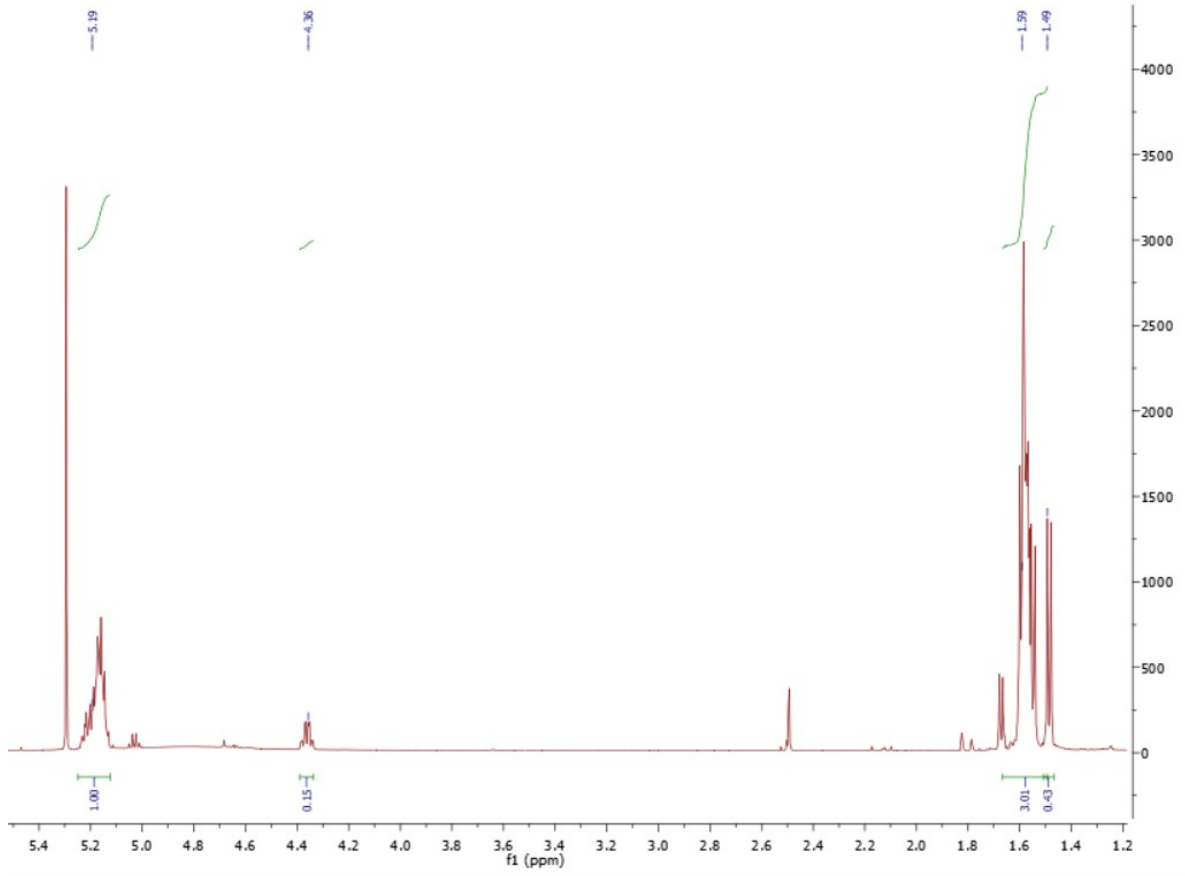

Figure S11: ^{1}H NMR (500 MHz, $CDCl_3$) spectrum of Entry 3 (Table 4).

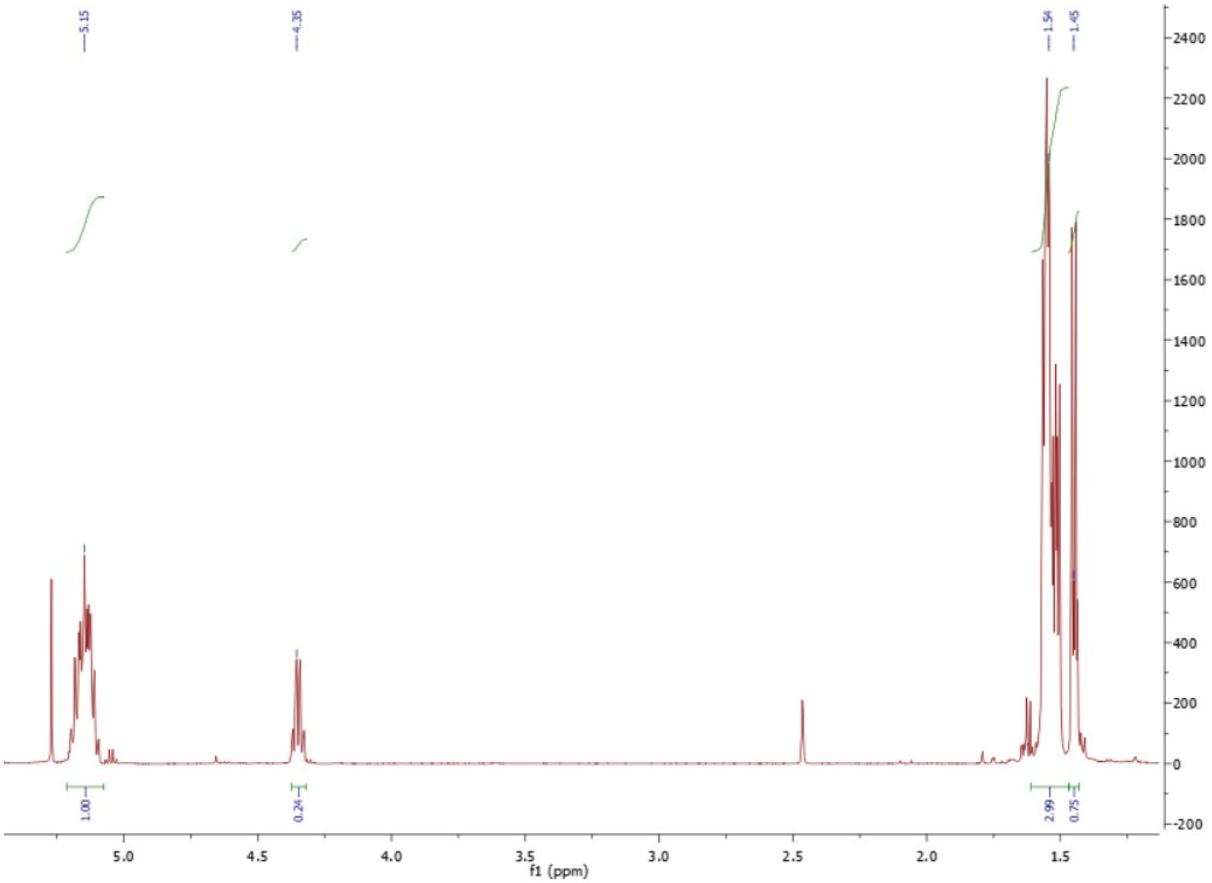

Figure S12: ^{1}H NMR (500 MHz, $CDCl_3$) spectrum of Entry 4 (Table 4).

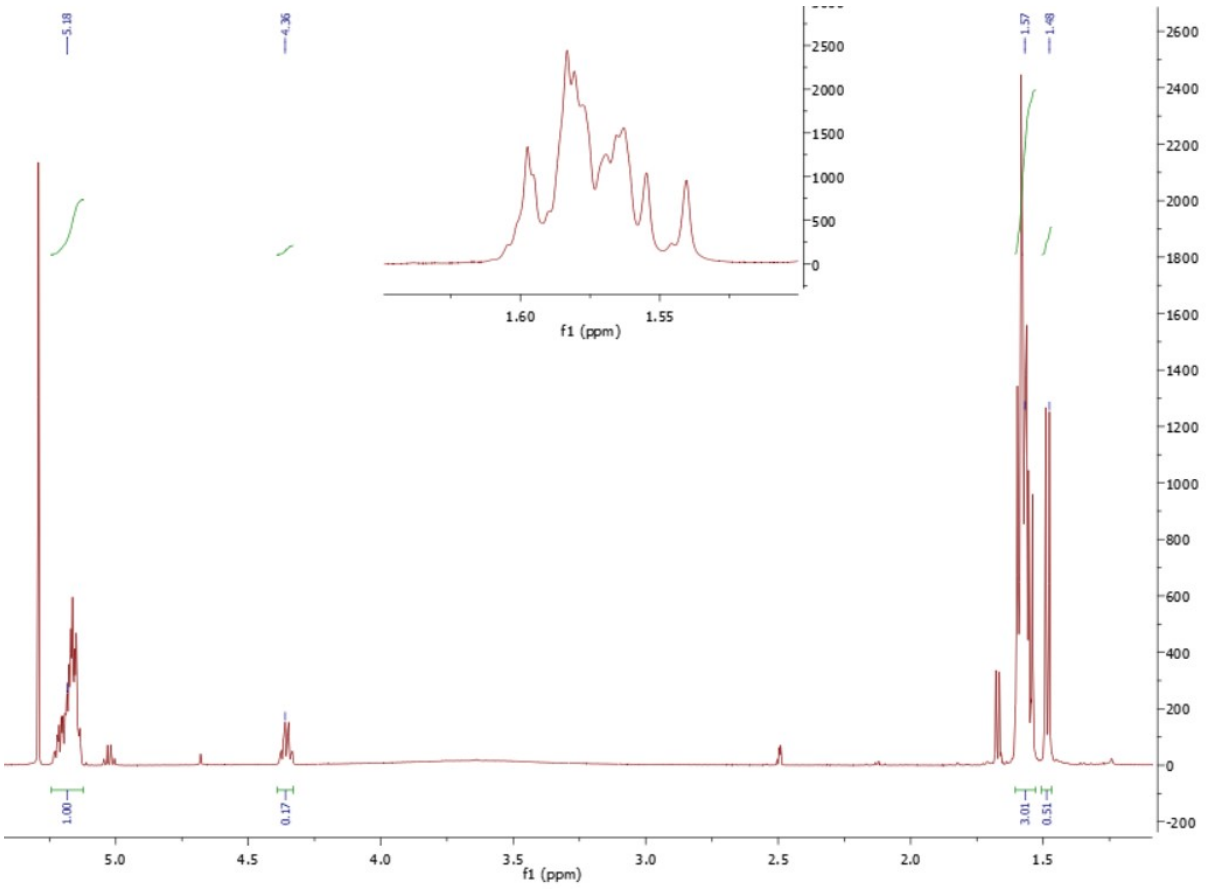

Figure S13: ^{1}H NMR (500 MHz, $CDCl_3$) spectrum of Entry 5 (Table 4).

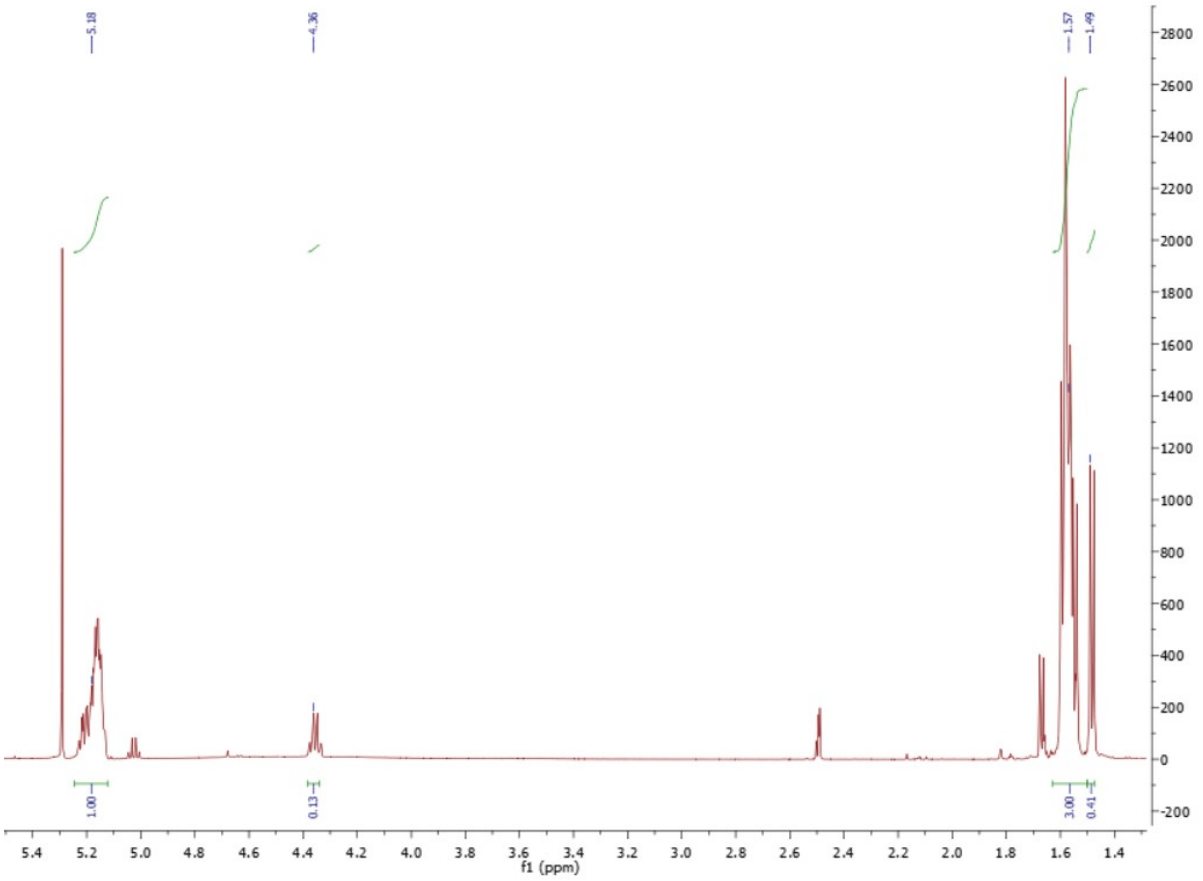

Figure S14: ^{1}H NMR (500 MHz, $CDCl_3$) spectrum of Entry 6 (Table 4).

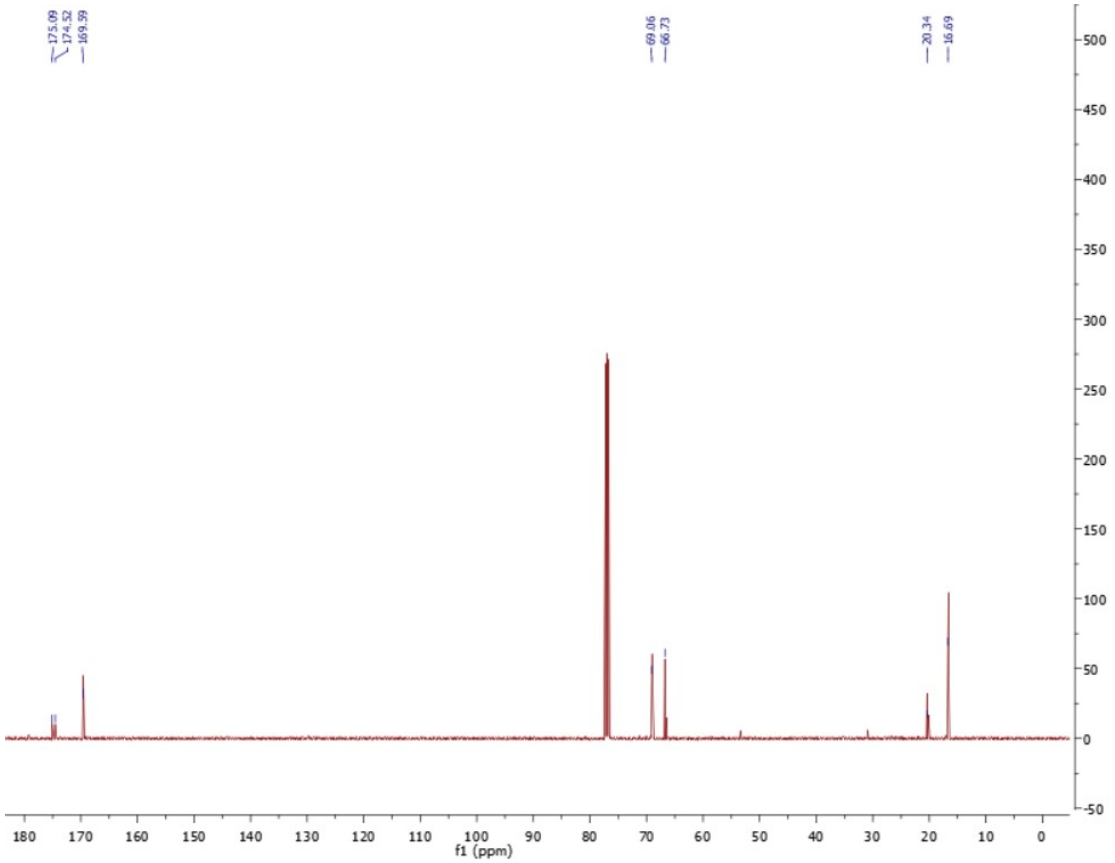

Figure S15: ^{13}C NMR (500 MHz, $CDCl_3$) spectrum of Entry 6 (Table 4).

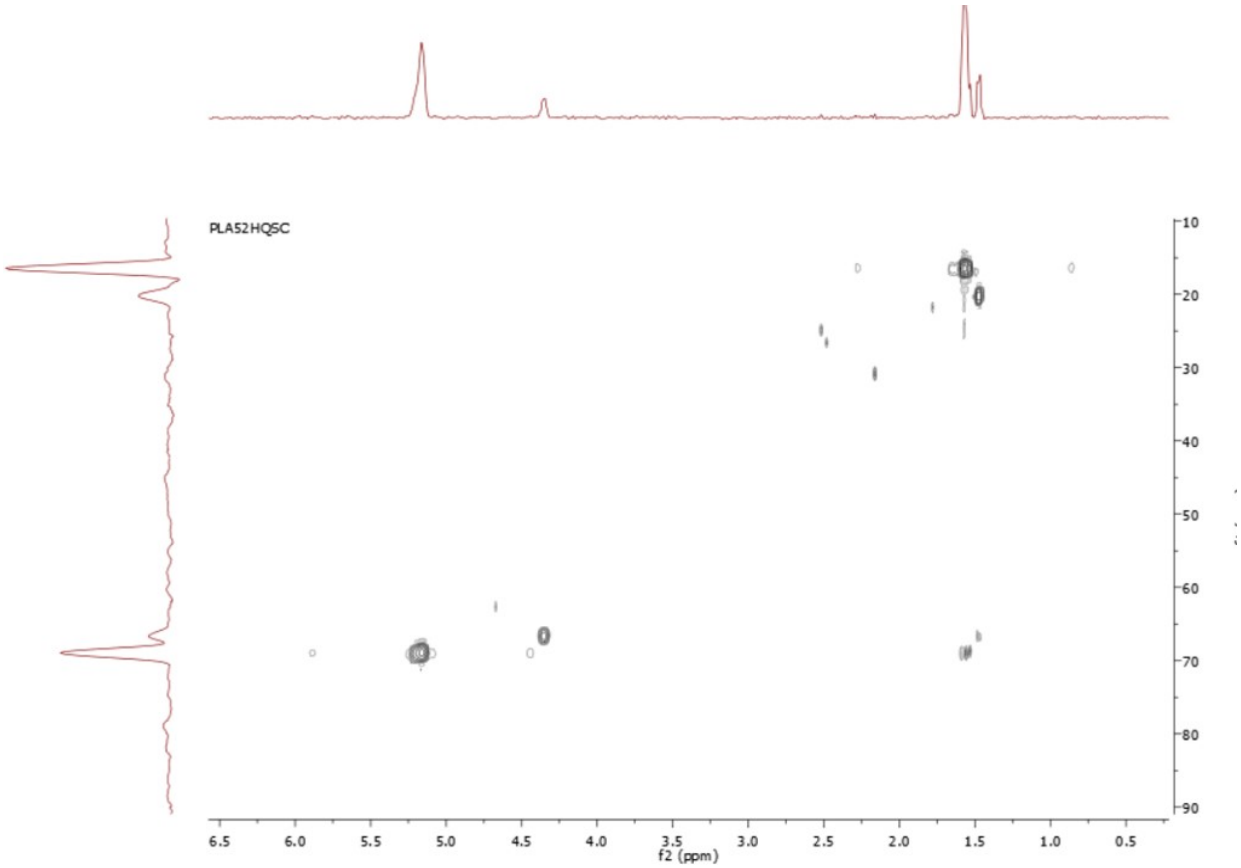

Figure S16: HSQC NMR (500 MHz, $CDCl_3$) spectrum of Entry 6 (Table 4).

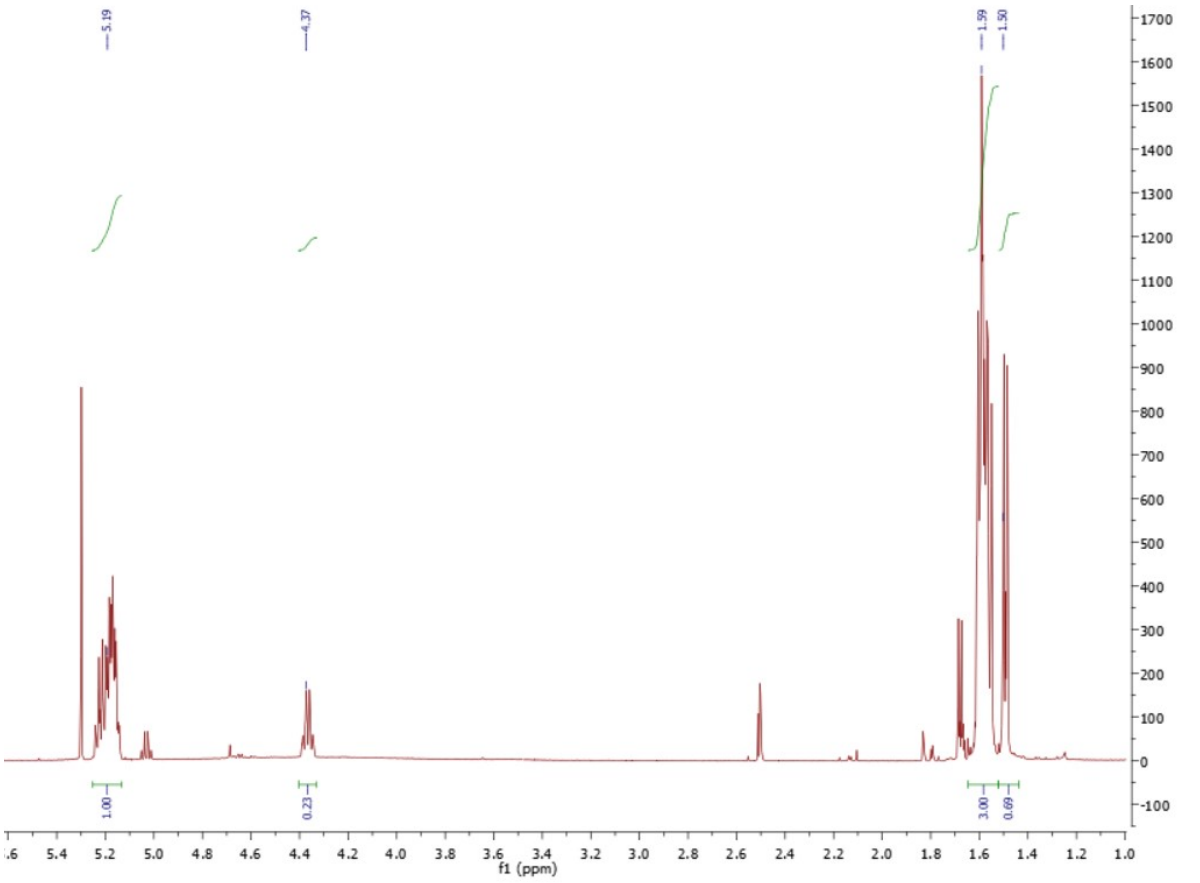

Figure S17: ^{1}H NMR (500 MHz, $CDCl_3$) spectrum of Entry 7 (Table 4).

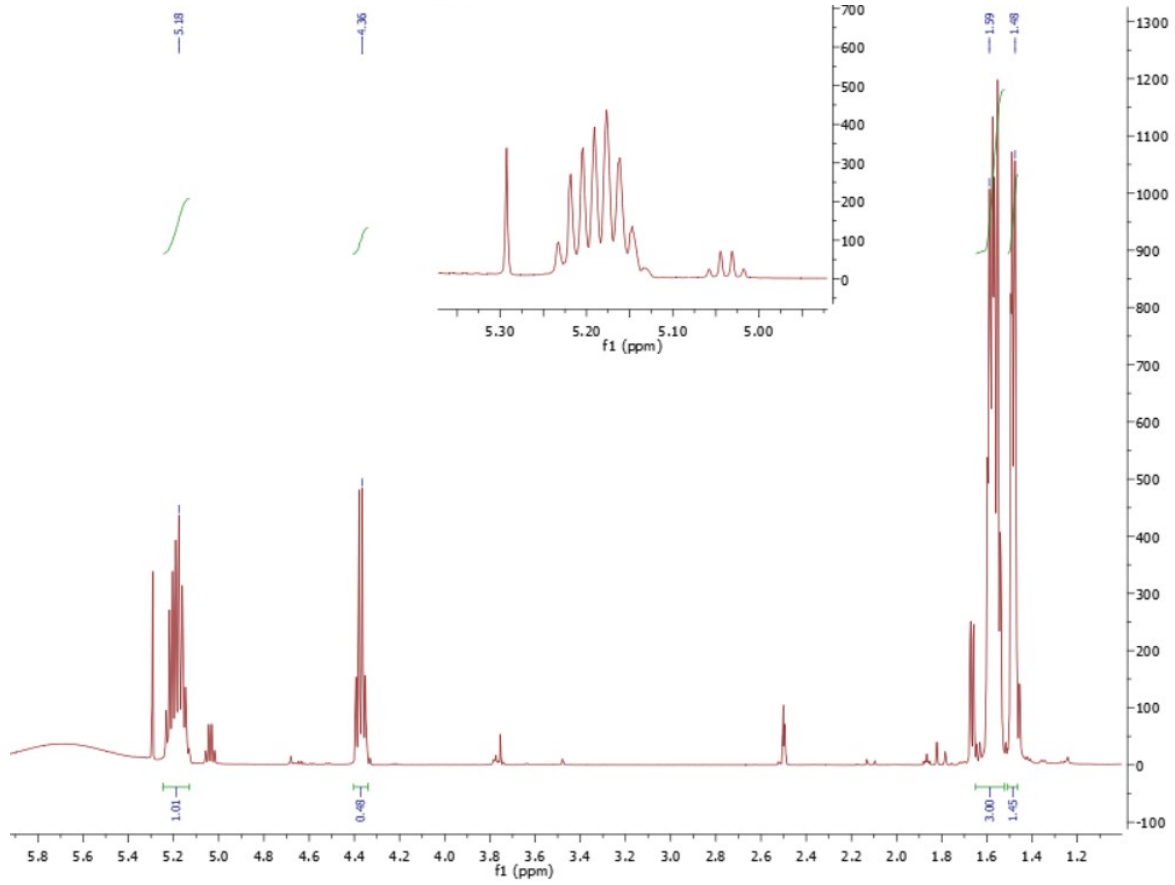

Figure S18: ^{1}H NMR (500 MHz, $CDCl_3$) spectrum of Entry 8 (Table 4).

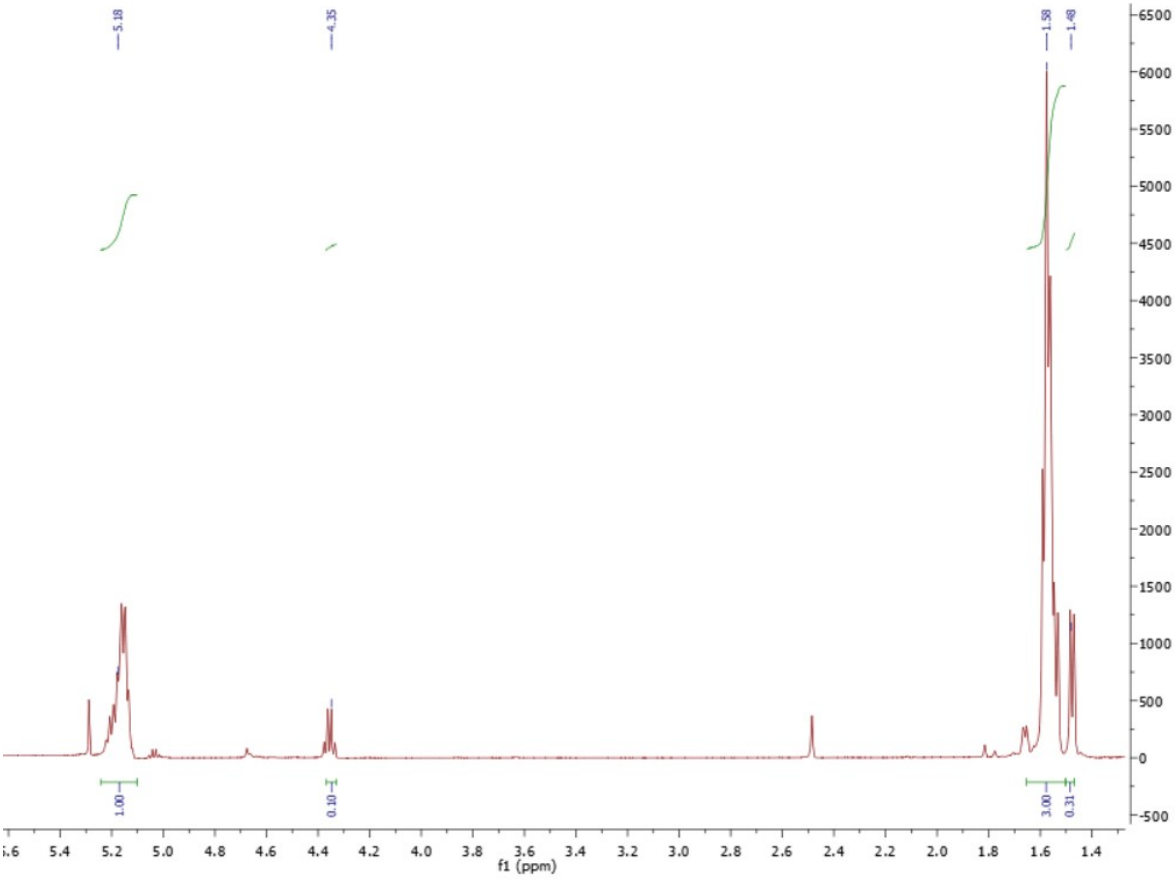

Figure S19: ^{1}H NMR (500 MHz, $CDCl_3$) spectrum of Entry 1 (Table 5).

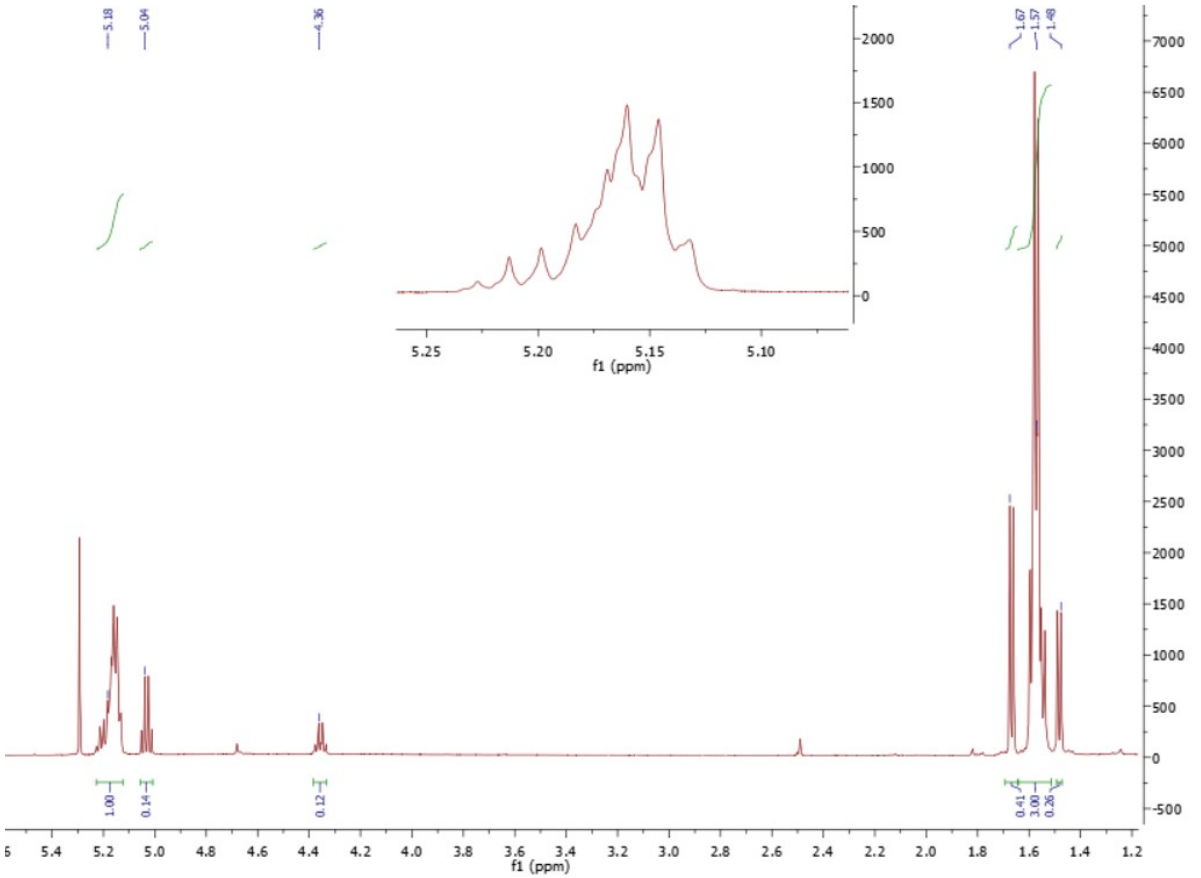

Figure S20: ^{1}H NMR (500 MHz, $CDCl_3$) spectrum of Entry 2 (Table 5).

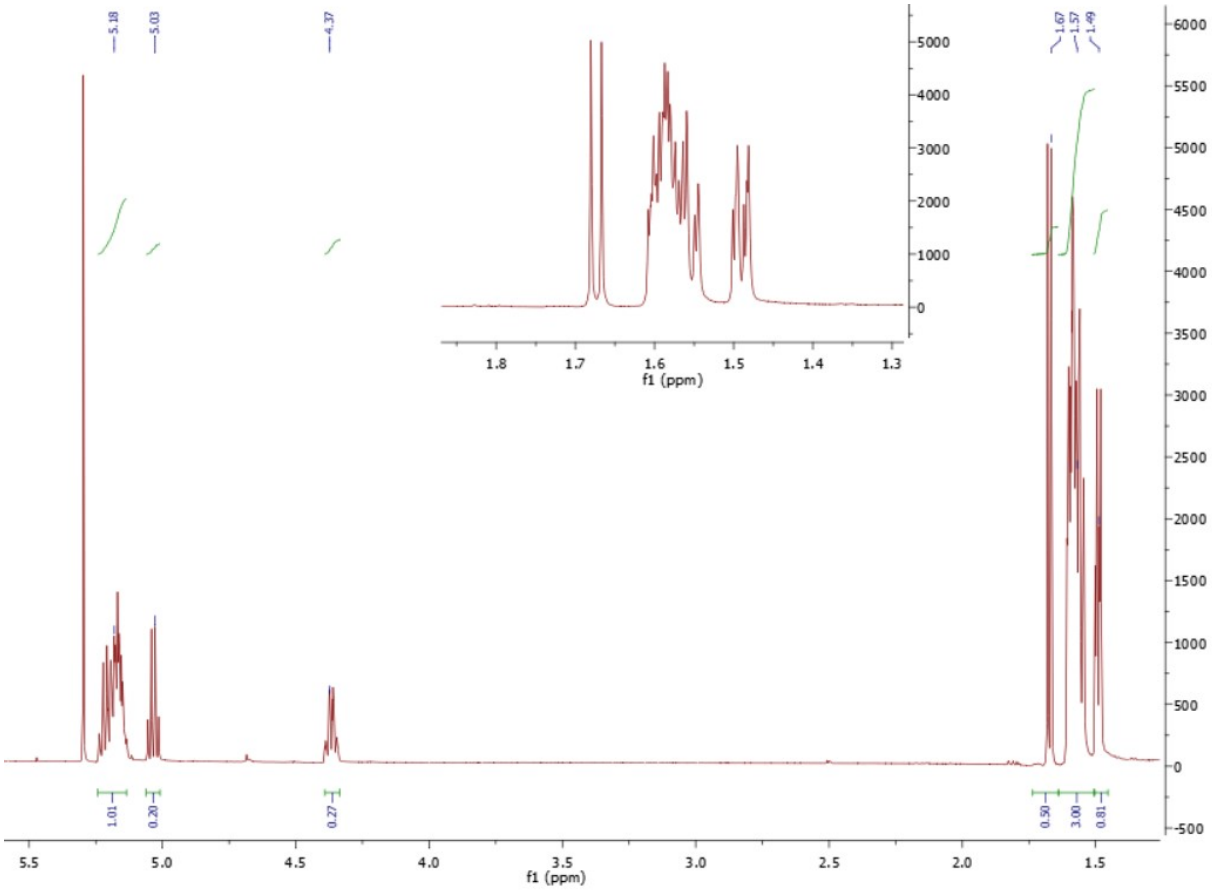

Figure S21: ^{1}H NMR (500 MHz, $CDCl_3$) spectrum of Entry 3 (Table 5).

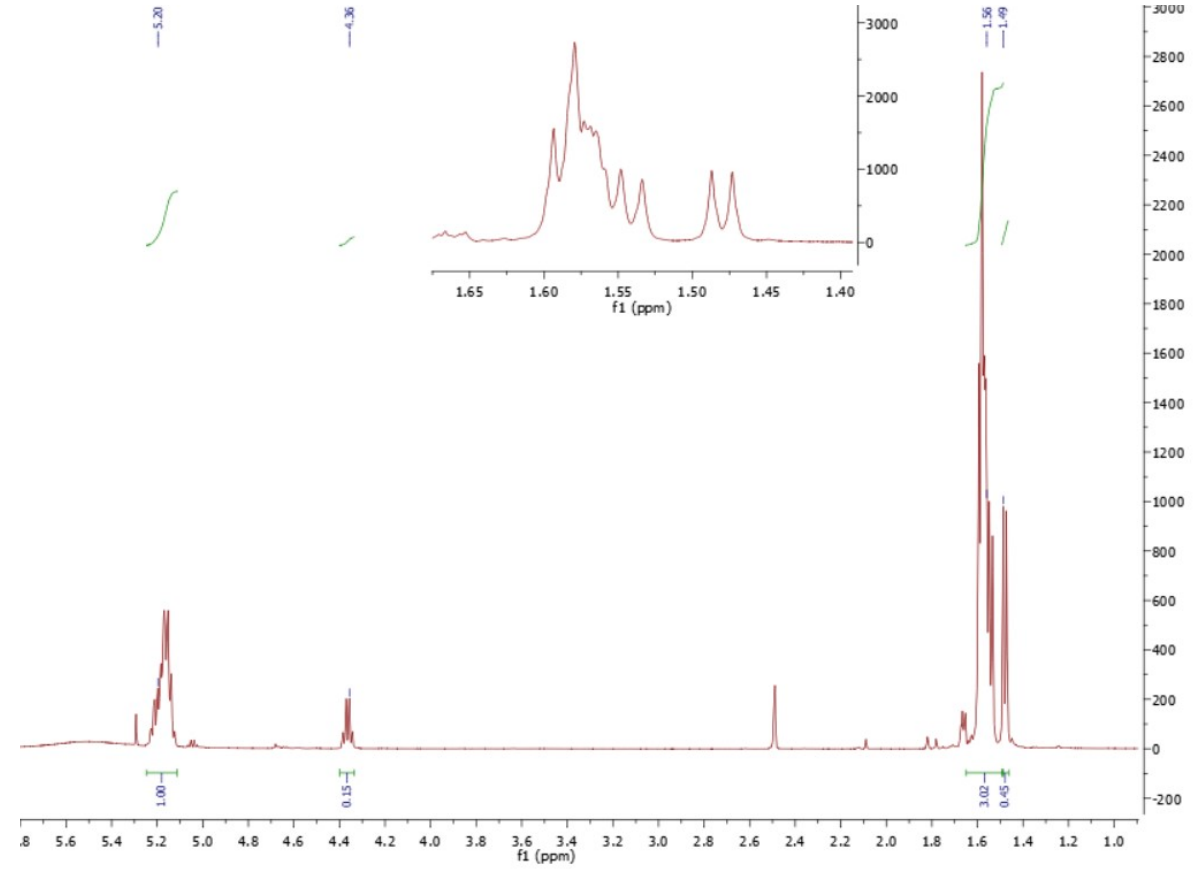

Figure S22: ^{1}H NMR (500 MHz, $CDCl_3$) spectrum of Entry 4 (Table 5).

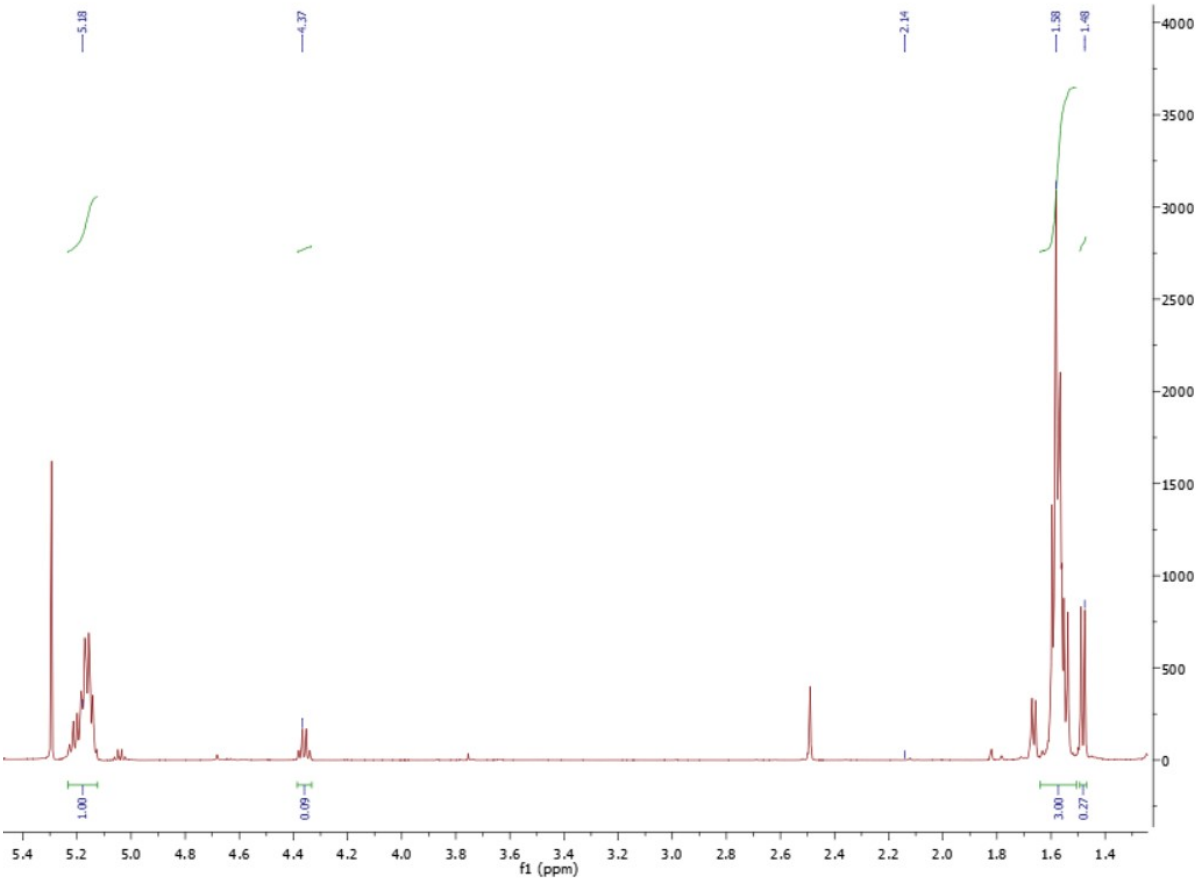

Figure S23: ^{1}H NMR (500 MHz, $CDCl_3$) spectrum of Entry 5 (Table 5).

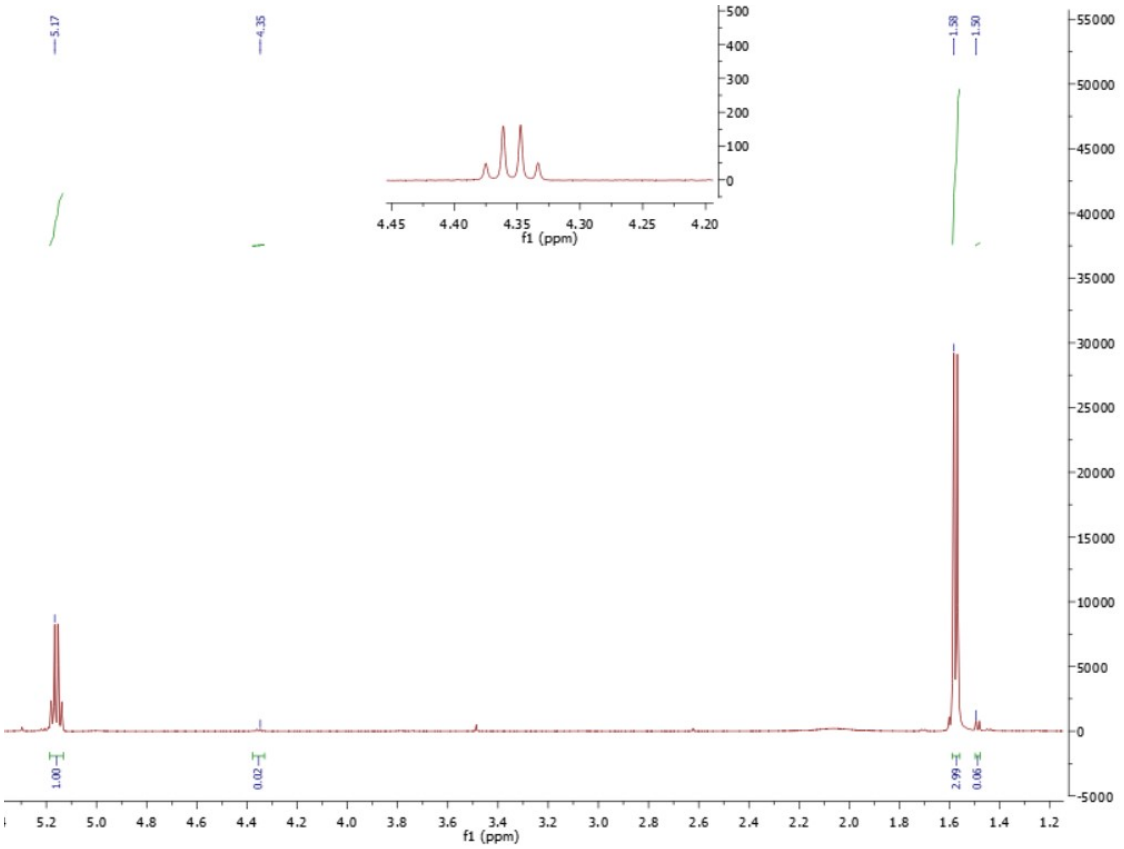

Figure S24: ^{1}H NMR (500 MHz, $CDCl_3$) spectrum of Entry 1 (Table 6).

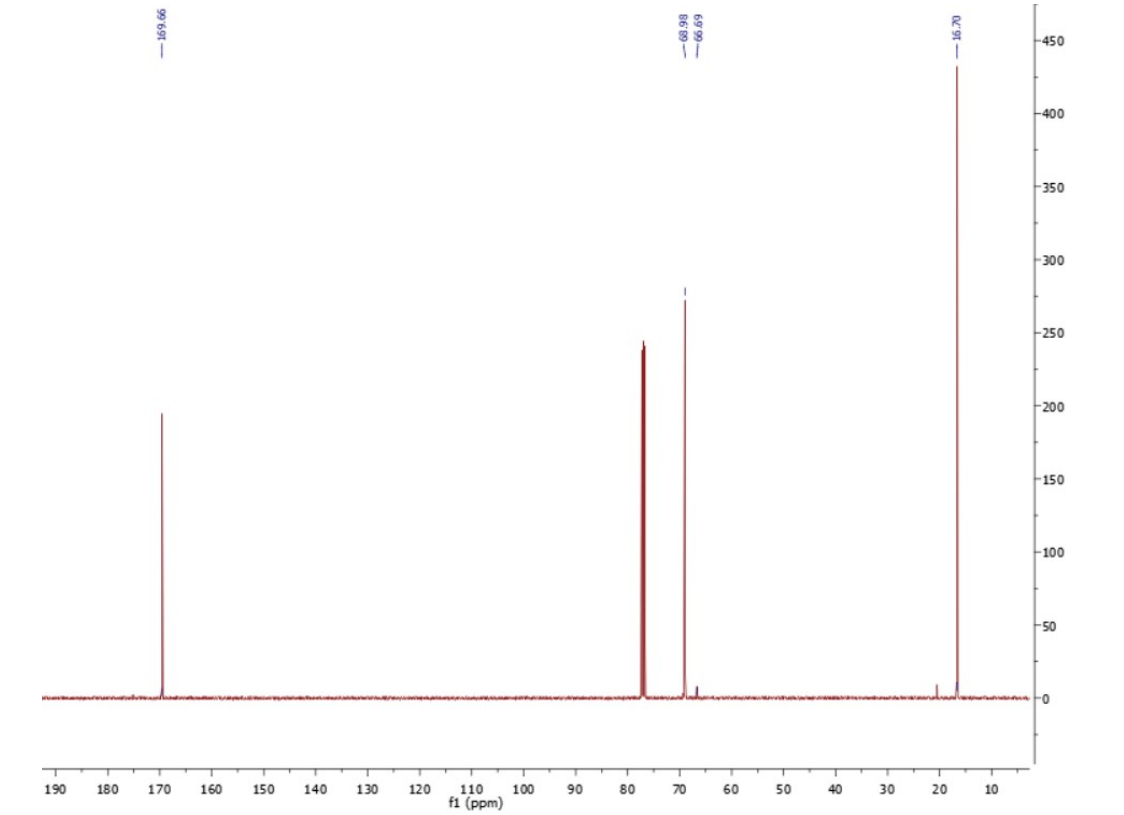

Figure S25: ^{13}C NMR (500 MHz, $CDCl_3$) spectrum of Entry 1 (Table 6).

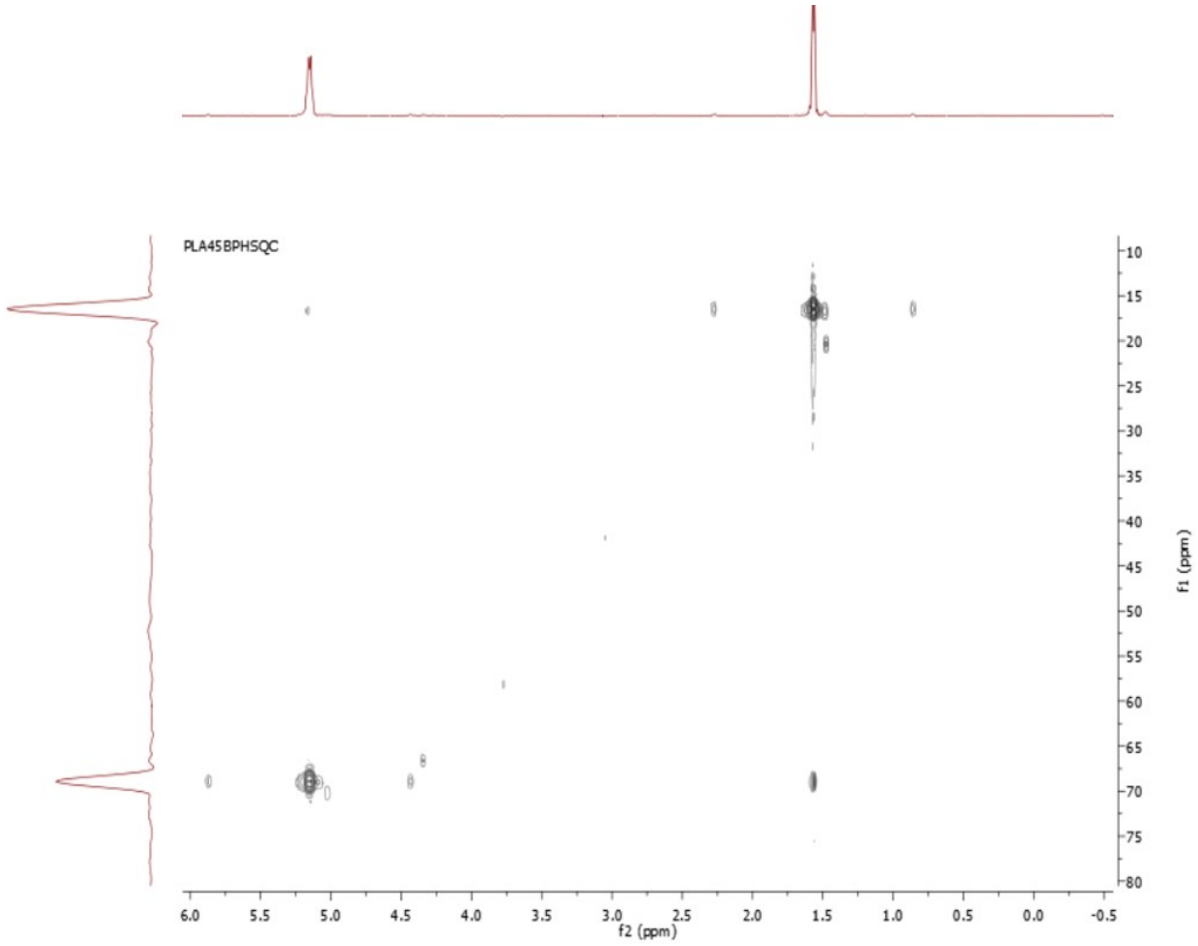

Figure S26: HSQC NMR (500 MHz, $CDCl_3$) spectrum of Entry 1 (Table 6).

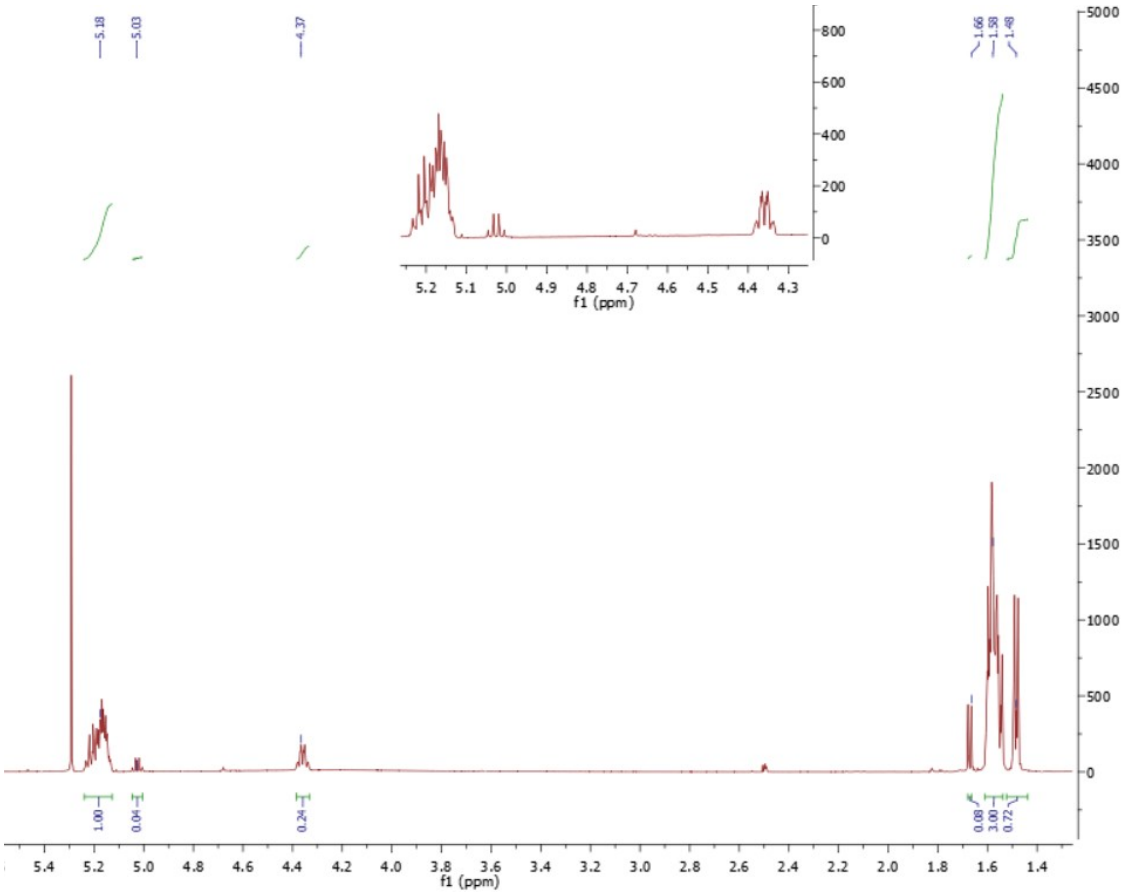

Figure S27: ^{1}H NMR (500 MHz, $CDCl_3$) spectrum of Entry 2 (Table 6).

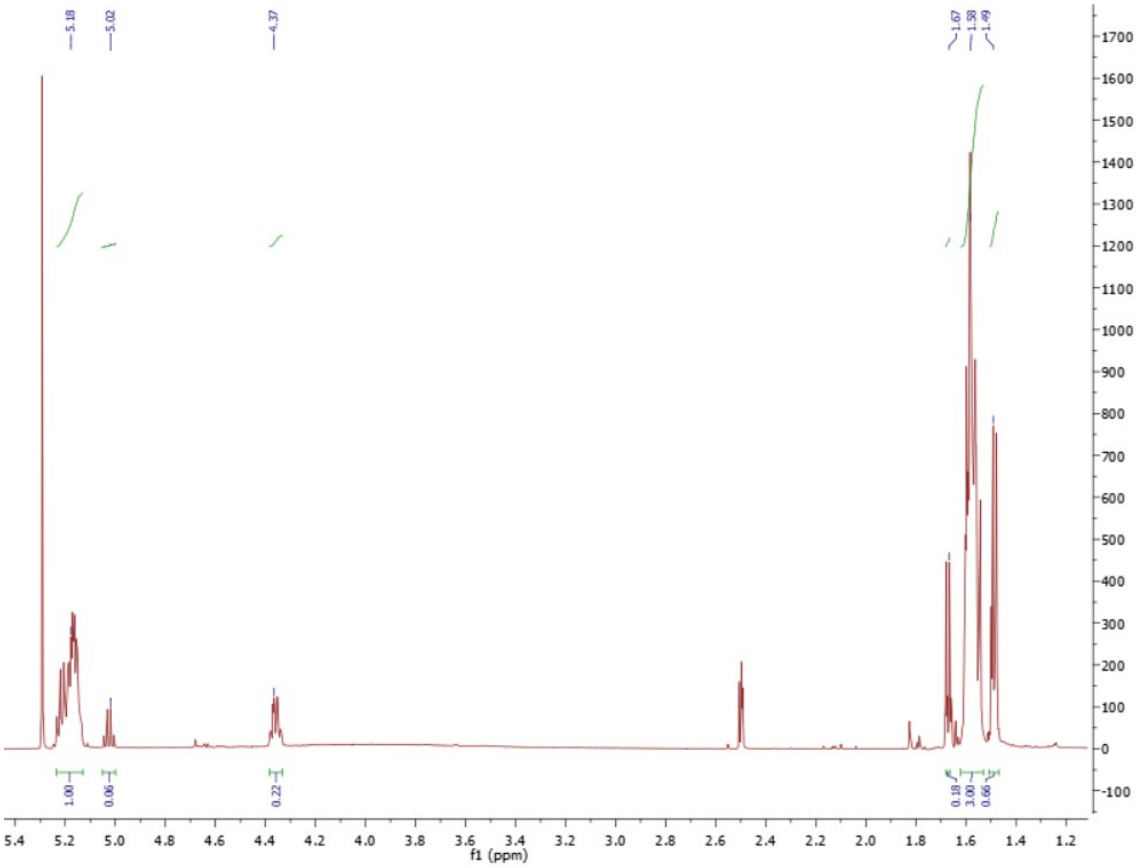

Figure S28: ^{1}H NMR (500 MHz, $CDCl_3$) spectrum of Entry 3 (Table 6).

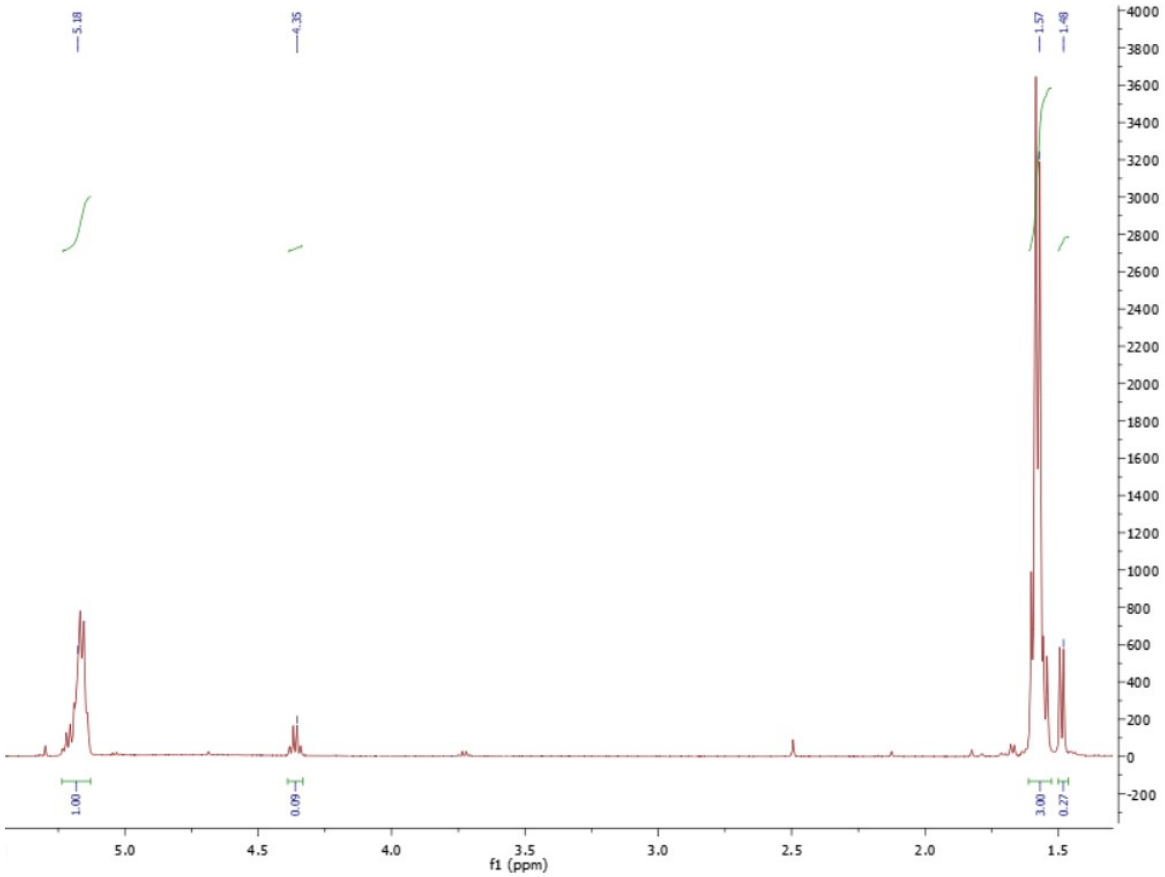

Figure S29: ^{1}H NMR (500 MHz, $CDCl_3$) spectrum of Entry 4 (Table 6).

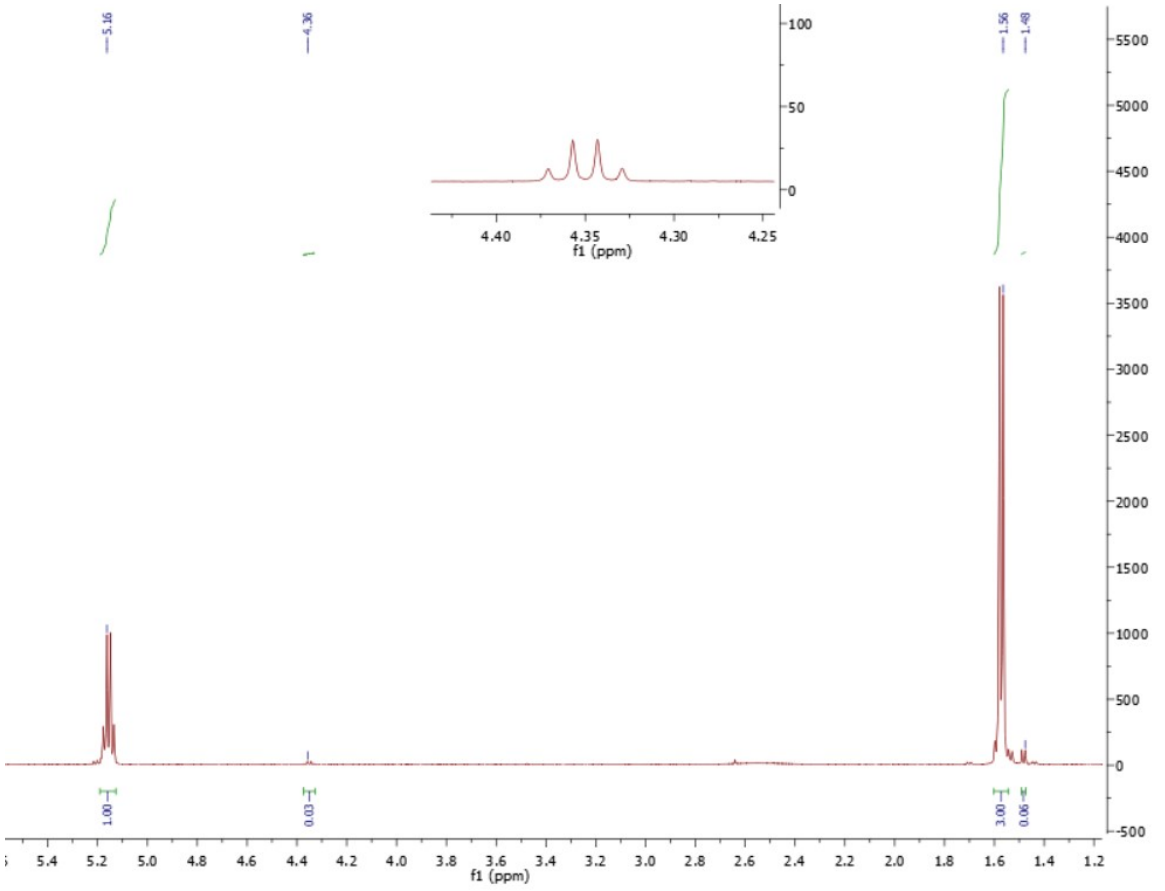

Figure S30: ^{1}H NMR (500 MHz, $CDCl_3$) Entry 6 (Table S1).

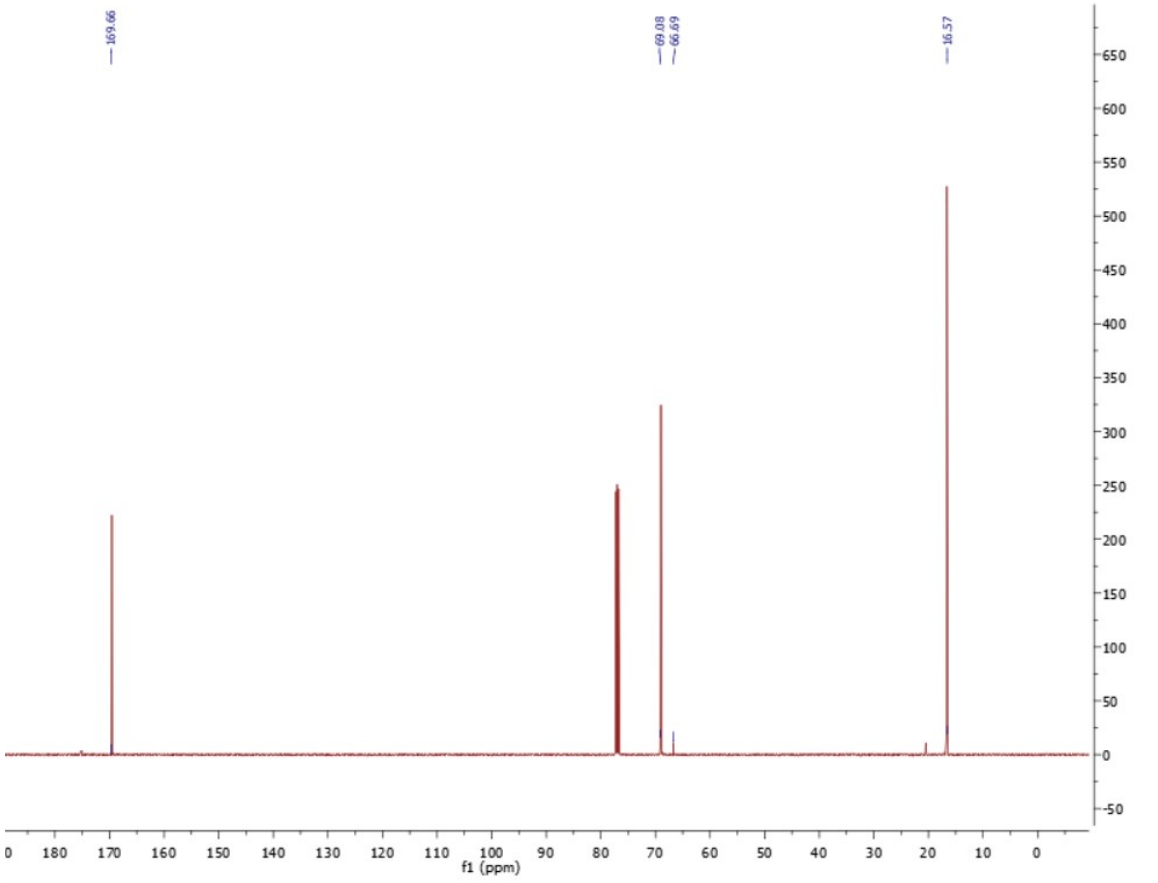

Figure S31: ^{13}C NMR (500 MHz, $CDCl_3$) spectrum of Entry 6 (Table S1).

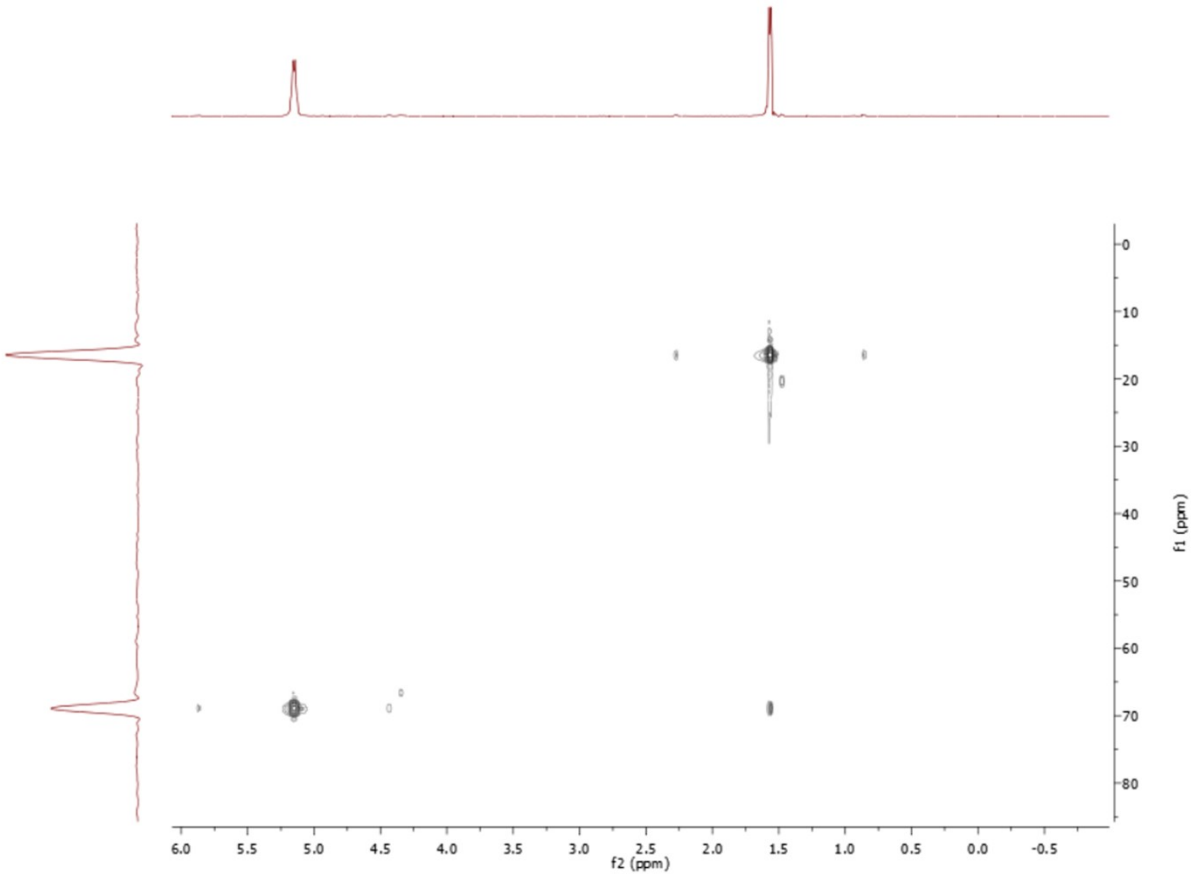

Figure S32: HSQC NMR (500 MHz, $CDCl_3$) spectrum of Entry 6 (Table S1).

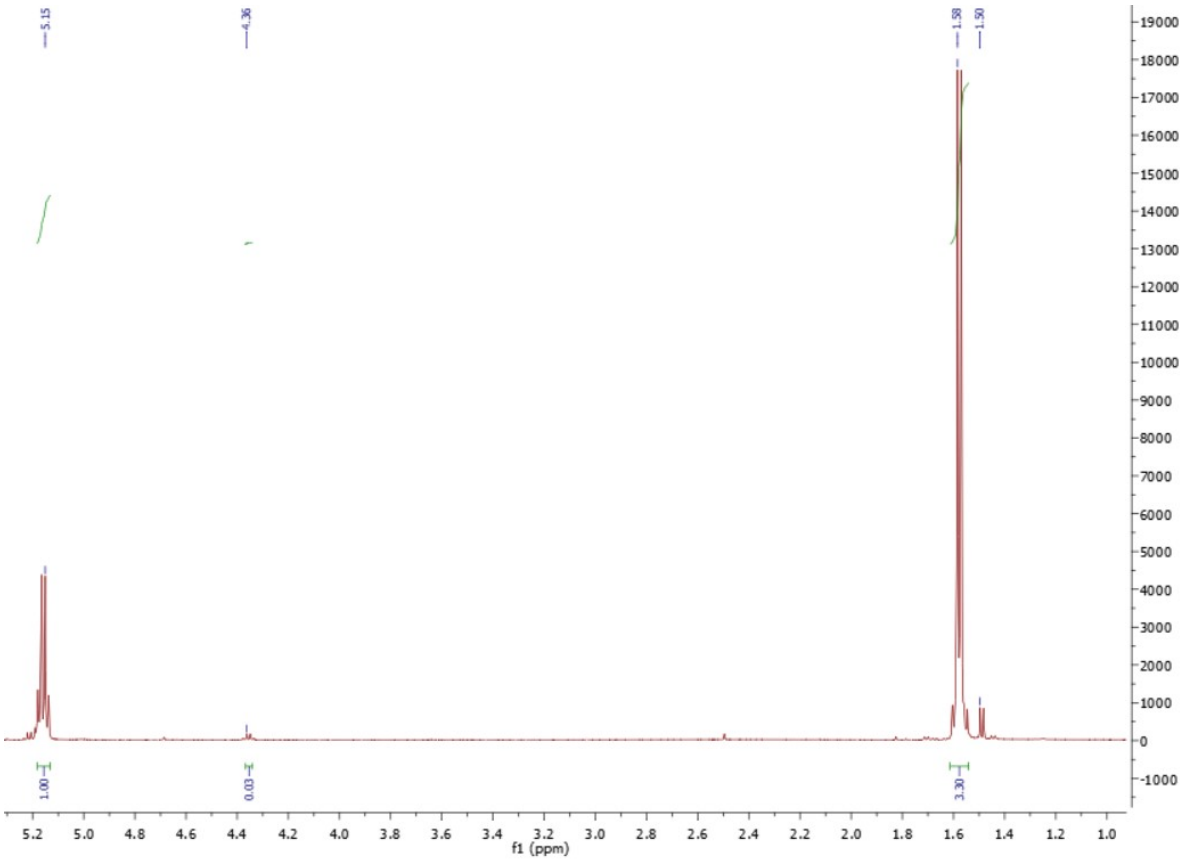

Figure S33: ^{1}HNMR (500 MHz, $CDCl_3$) spectrum of PLLA, after photodegradation reaction.

S5. WAXD Results

The crystalline structures of the two PLA samples were analyzed using wide-angle X-ray diffraction (WAXD). The corresponding results for PLLA (**Entry 1, Table 8**) and PDLLA (**Entry 2, Table 8**) are presented in Figure S34A and S34B, respectively. It is well known that, depending on the crystallization conditions, PLA can form one of several polymorphs: α-, α′-, β-, or γ- form [1]. Under typical melt or solution crystallization conditions, PLA predominantly crystallizes into the α-form, which is the most stable and commonly observed polymorph. This form features a 10_3 helical chain conformation, with two chains arranged in an orthorhombic unit cell [2]. Zhang et al. [3] identified a disordered crystalline structure, known as the α′-form, which typically develops at low crystallization temperatures. The β-form arises by stretching the α-form under conditions of high temperature and significant drawing ratios. In contrast, the γ-form is generated through epitaxial crystallization, a process first described by Cartier et al. [4].

Significant differences in the WAXD patterns are observed between PLLA and PDLLA. PLLA (Figure S34A) displays the characteristic diffraction peaks of α-form that are identified in the region between 2θ values of 10 and 35°. The material has a crystallinity of 91.5%. Conversely, PDLLA exhibits an amorphous structure, as evidenced by a broad scattering pattern resulting from the overlap of two halos centered at 2θ values of 16.5° and 20.4°. This behavior is like that observed in PET [5], and has also been reported for PLA, suggesting the presence of two distinct interchain distances [6].

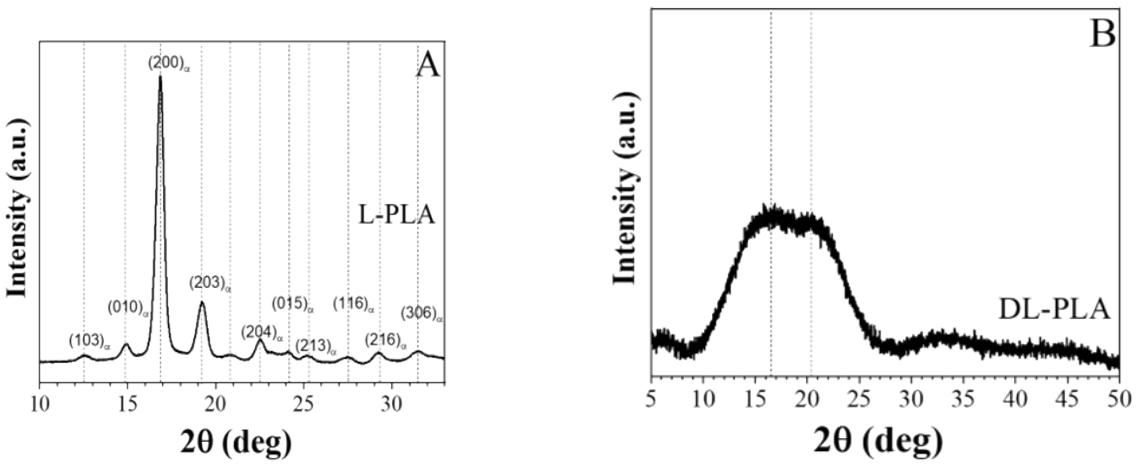

Figure S34: WAXD patterns of (A) PLLA and (B) PDLLA.

S6. FT-IR analysis

FTIR analysis was performed on **Entry 6, Table 4** and **Entry 1, Table 6 and Entry 2, Table 8** (as KBr pellets). FTIR spectrum of commercial pure PLLA (as KBr pellets) was compared with FTIR spectra of Entry 6 (Table 4), Entry 1 (Table 6) and Entry 2 (Table 8) (Figure S35-S40). Figure S35 compares FT-IR spectrum of Commercial PLLA and OligoLA with low molecular weight **(Entry 6, Table 4, Mn = 475 Da)**. Figure S38 compares FT-IR spectrum of Commercial PLLA and PLLA with medium-high molecular weight (**Entry 1, Table 6, Mn = 7999 Da).** Finally, Figure S40 compares FT-IR spectrum of Commercial PLLA and PDLLA (**Entry 2, Table 8, Mn = 3123 Da)**.

The comparisons reveal two distinctive spectral differences in intensity of bands: the stretching vibrations of hydroxyl groups *ν*(OH), the asymmetric stretching vibration of carboxyl groups ν_{as}(COO). The typical stretching vibration peak of O−H of hydroxyl groups are evident at 3485.93 cm^{-1} for **Entry 6, Table 4** (Figure S35) and less evident at 3509.11 cm^{-1} for **Entry 2, Table 8** (Figure S39) and almost absent at 3649,51 cm^{-1} for **Entry 1, Table 6** (Figure S37). For Commercial PLLA the peak of O−H of hydroxyl groups disappears. The ν(OH) broad band is the result of hydrogen bond formation by the OH (sub) groups of carboxyl groups and alpha hydroxyl groups [7]. For this reason, going from PLA to about 7999, to 3173 up to 475 Da, the band widens. Moreover, the asymmetric stretching vibration of the carboxylate groups, ν_{as}(COO), located around ~1630 cm^{-1}, tends to increase in intensity with increasing polymer molecular weight and, consequently, crystallinity. In the case of racemic PLA, the ν_{as}(COO) peak appears at 1635,92 cm^{-1} (Figure S39), which is consistent with the highly amorphous nature of the material. A similar behavior is observed for **Entry 6, Table 4**, where the signal is detected at 1639,39 cm^{-1} (Figure S35); in this case, the presence of the band is attributed to the low molecular weight of the sample, which reduces its crystallinity. Conversely, in the polymer **Entry 1, Table 6** (Figure S37), the signal is less intense and appears at 1620,46 cm^{-1}. This is consistent with the higher molecular weight of the sample, which leads to greater crystallinity and therefore a less pronounced ν_{as}(COO) band. Finally, in commercial PLA, the ν_{as}(COO) peak is not observed, as shown in Figures S36, S38, and S40.

The polymerization of mixtures of L- and D-lactic acid leads to PDLLA or racemic PLA with a random distribution of the L- and D-lactyl units. In this case, the amorphous polymer in the absence of crystalline phases caused a broadening of lines in the IR spectrum (Figure S39). The characteristic signals, such as the C=O stretching band region at ~1750 cm^{-1}, the CH_3, CH bending, and C-O-C stretching band region at 1500-

1000 cm^{-1}, and the skeletal stretching and CH_3 rocking band region of 970-850 cm^{-1} are evident. In this latter spectral region, the bands at 951.15 and 867.11 cm^{-1} observed in the IR spectrum of the racemic sample reflect the amorphous state typical of racemic PLA (Figure S39).

As the number of crystalline domains increases, two main changes occur: the band at 951.15 cm^{-1} in the racemic sample shifts to 919.43 cm^{-1} in the more crystalline polymer, and its intensity decreases (Figure S37). the band at 867.11 cm^{-1}, also characteristic of the racemic sample, shifts to 870.58 cm^{-1} in the chiral polymer, while retaining approximately the same intensity (Figure S39). These shifts confirm the higher crystallinity of the chiral samples compared to racemic PLA.

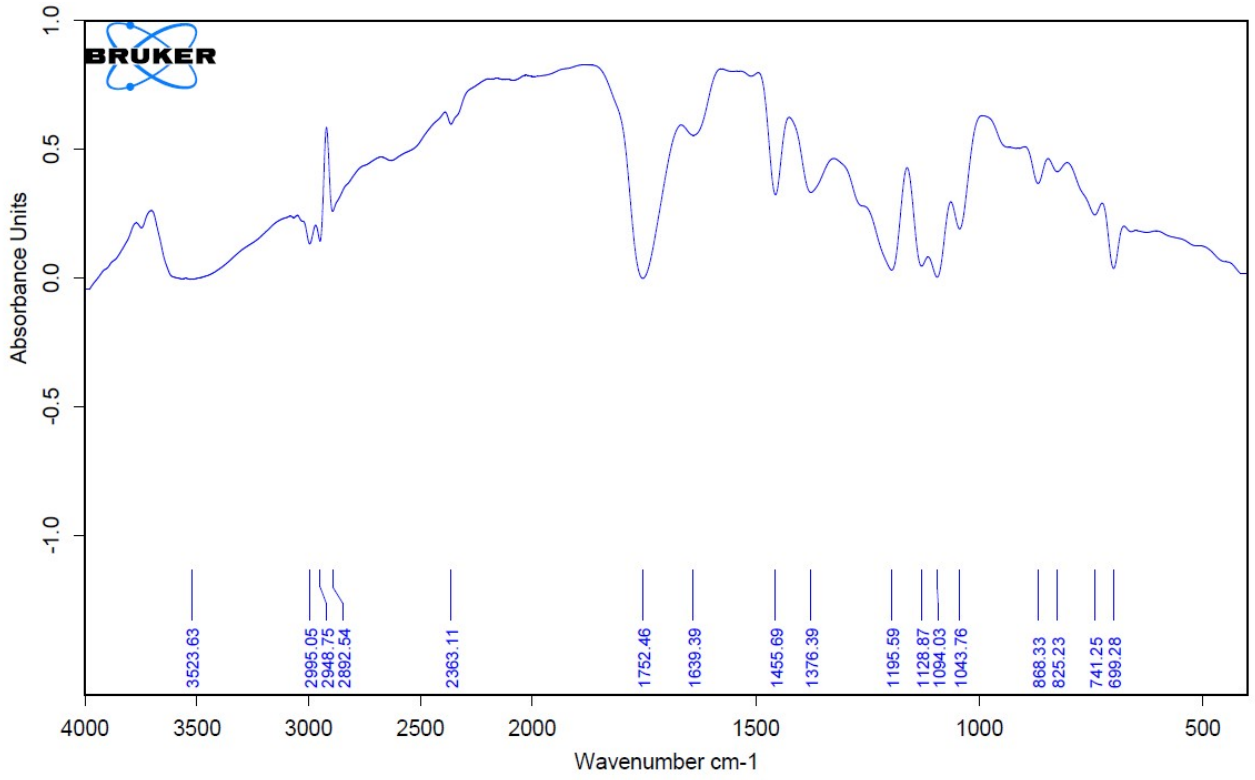

Figure S35: FTIR spectra of OligoLA Entry 6, Table 4, Mn = 475 Da.

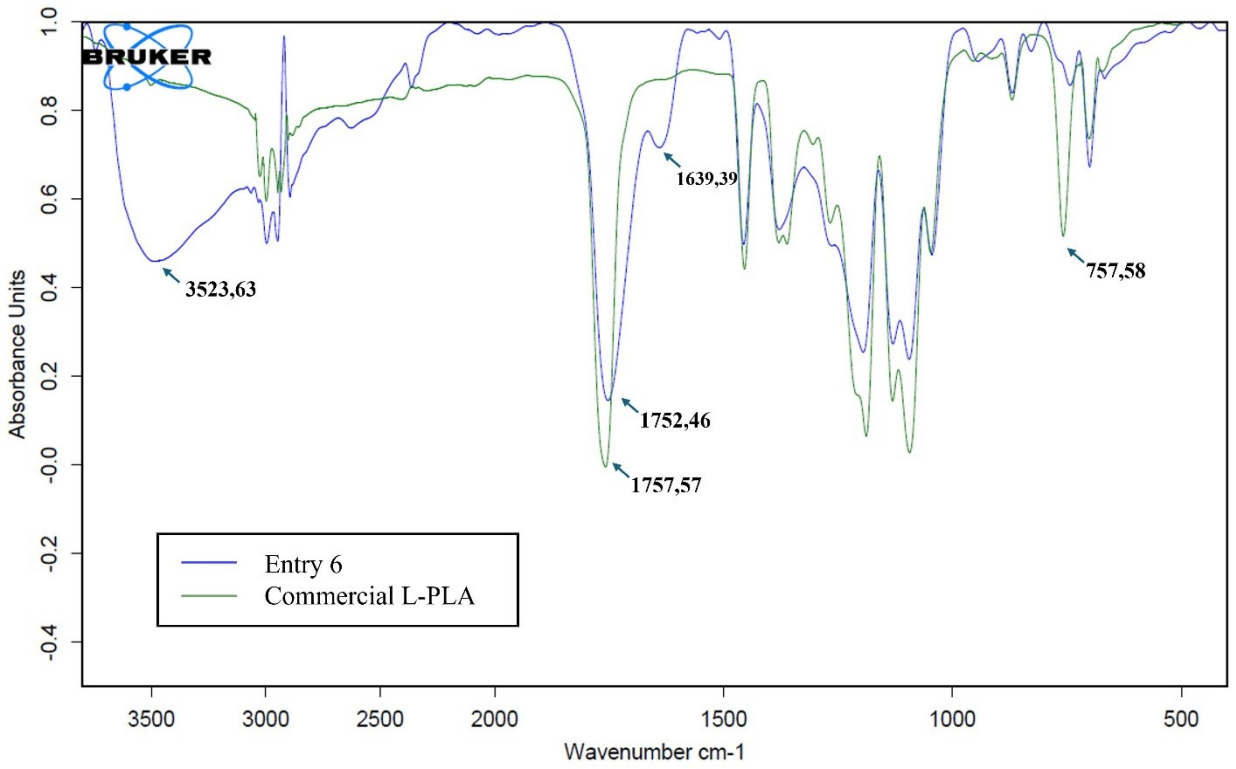

Figure S36: FTIR spectra of commercial PLLA (green) and spectra of OligoLA Entry 6, Table 4, Mn = 475 Da (blue).

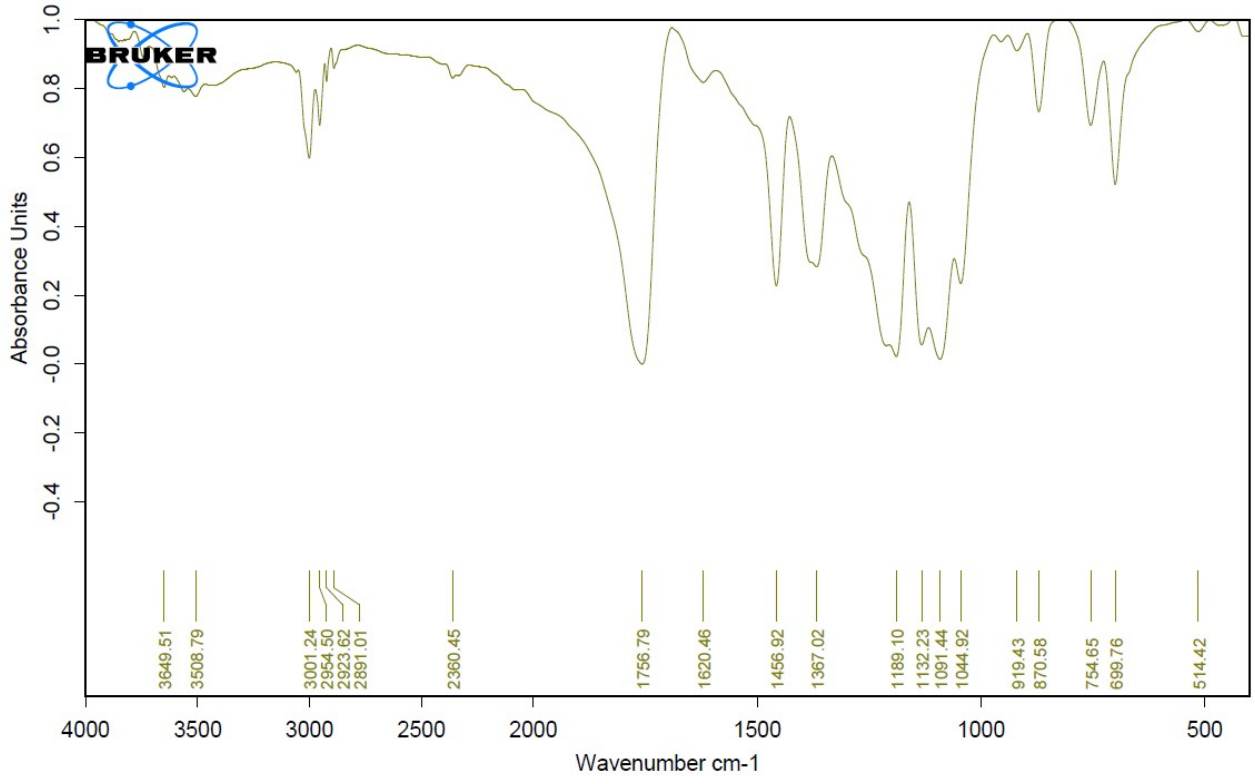

Figure S37: FTIR spectra of PLLA Entry 1, Table 6, Mn = 7999 Da.

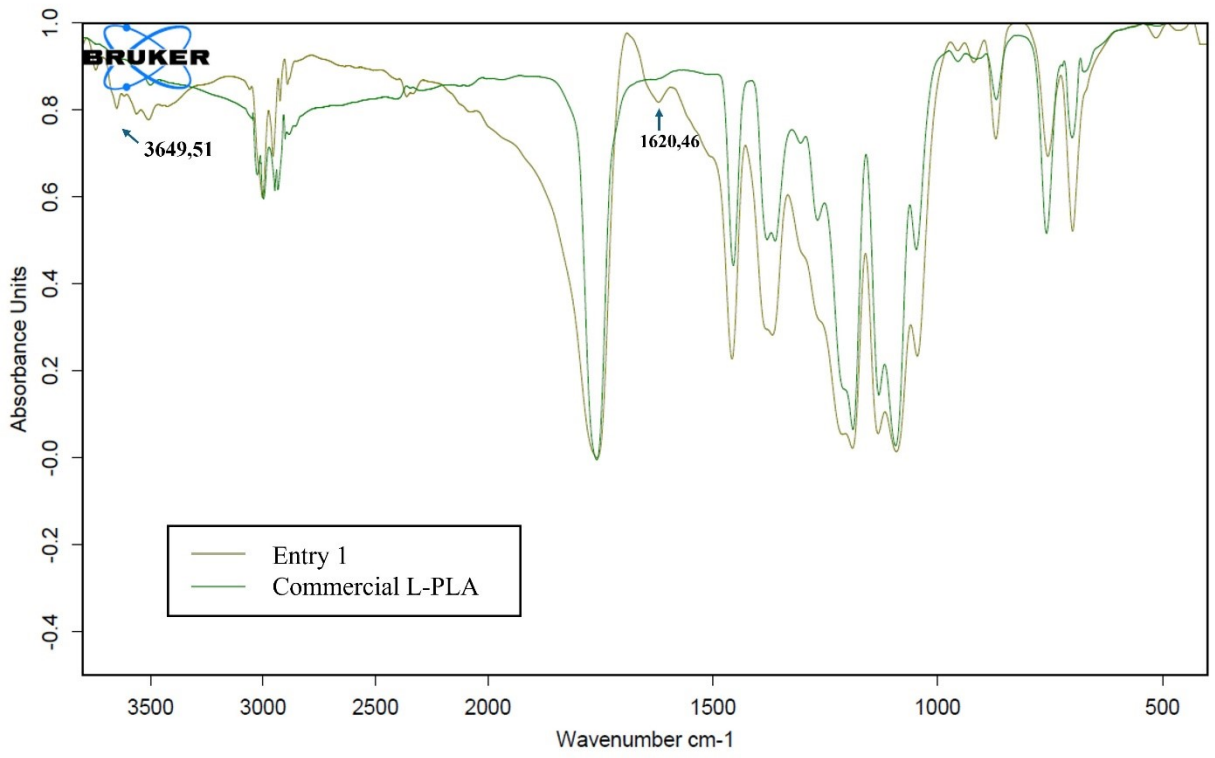

Figure S38: FTIR spectra of commercial PLLA (green) and PLLA Entry 1, Table 6, Mn = 7999 Da (light-green).

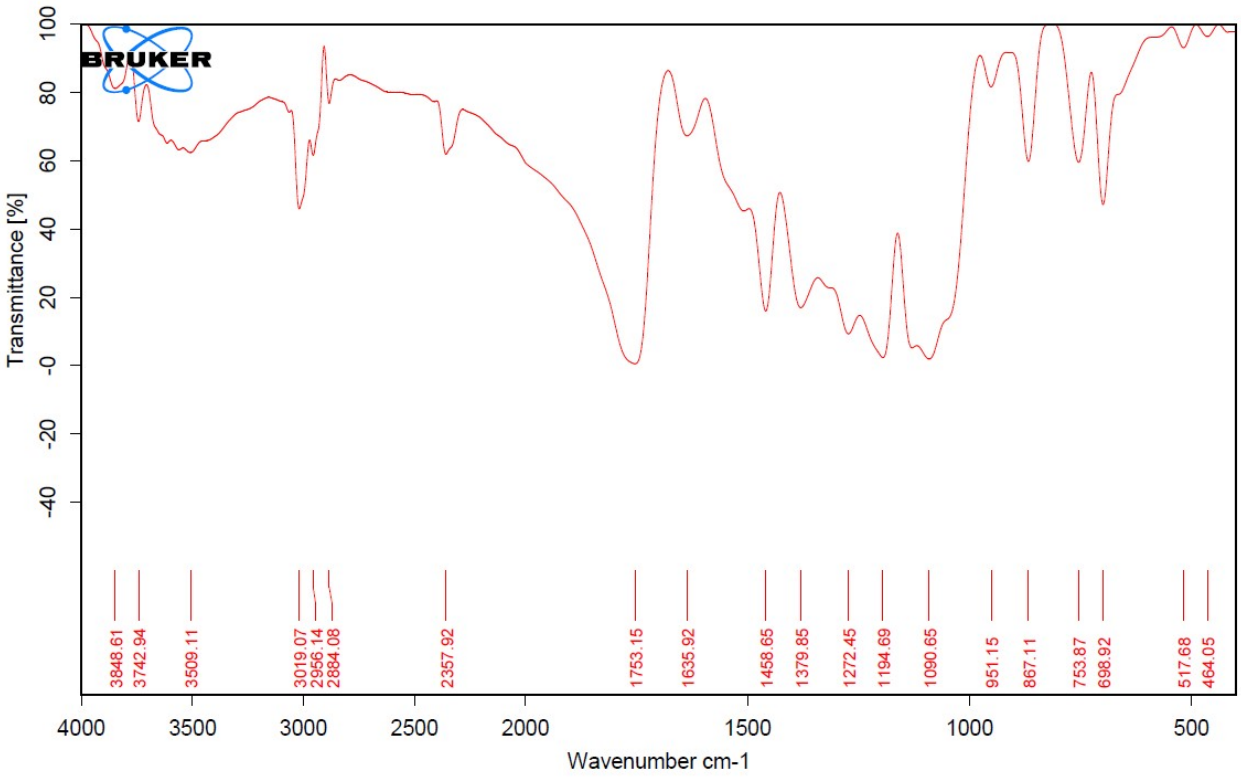

Figure S39: FTIR spectra of racemic PLA Entry 2, Table 8, Mn = 3123 Da (orange).

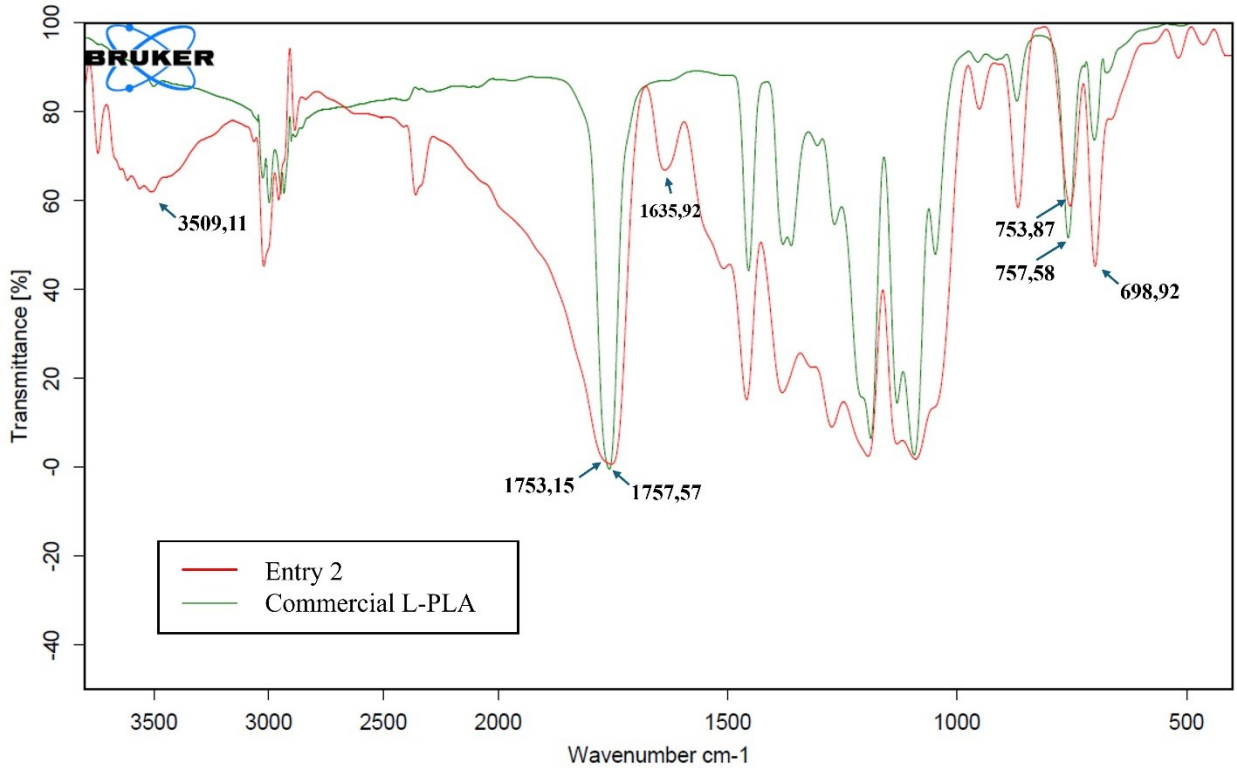

Figure S40: FTIR spectra of commercial PDLLA (green) and racemic PLA Entry 2, Table 8, Mn = 3123 Da (red).

S7. Thermal stability and photodegradation

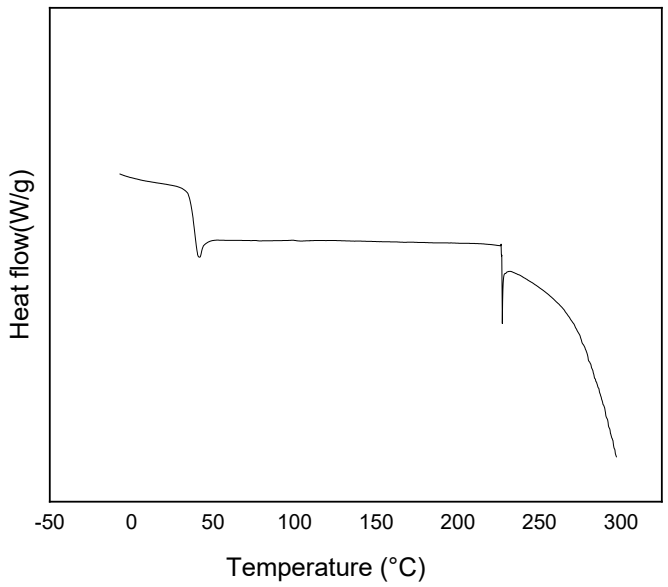

Figure S41: DSC curves of the second heating scan of the PDLLA sample.

Photostability was also evaluated using the sample with the highest molecular weight among those synthesized (**Entry 1, Table 6**). Photostability tests were performed on a 100 mg portion of the polymer. When positioned

7 cm from the IR lamp, the material initially showed no visible changes. After approximately 3 hours of irradiation, it gradually transformed into a transparent liquid, indicating the onset of melting. Upon removal from the light source, the sample immediately reverted to an opaque solid, suggesting that the observed phase change was purely thermal.

The NMR spectrum recorded after 5 hours of irradiation was identical to that of the untreated polymer (Figure S33), confirming the absence of any detectable degradation or secondary polymerization processes. Overall, these results demonstrate that **Entry 1** maintains its structural integrity under the applied irradiation conditions and can be considered photostable.

S8. Stereochemical investigation: Optical specific rotation at 589 nm *vs* GPC molecular weights [*Mn*(GPC)]

The correlation between the molecular weight of chiral PLLA and its specific optical rotation measured at 589 nm was investigated for different PLA samples obtained in this work (Table S7). The specific optical rotation was determined by preparing solutions of each PLA sample in 2 mL of CH_2Cl_2. The measured values were compared with that of a commercial PLLA sample (Mn = 32100 Da), used as a reference and dissolved under the same conditions.

All the analyzed samples, synthesized from the L-AL monomer, exhibited levorotatory behavior, as expected. Specifically, all polymers showed negative specific rotation values. Furthermore, the magnitude of the specific optical rotation increased in absolute value with increasing molecular weight: from –89° for an oligomer with Mn = 475 Da, to –149.6° for a polymer with Mn = 5313 Da, and up to –153° for the commercial polymer with Mn = 32100 Da (Table S7 and Figure S42).

The results show that there is a linear increase of the molar rotation with molecular weight. On the other hand, the specific rotation shows an evident increase for small molecular weights reaching a saturation for higher molecular weights. This shows that increase in physical properties specific rotation with molecular weights reaches a saturation value at higher degree of polymerization.

Table S7. Specific optical rotation compared with molecular weight

Catalyst	Mn (Da)	$[\alpha]^D$ (°)	Molar rotation [b] ($*10^4$)
//	32100[c]	-153	-491,13
$Sc(OTf)_3$	5313	-149,59	-79,48
PTSA	4241	-144.50	-61,28
$Zn(OTf)_2$	1903	-119,58	-22,75
$Sc(OTf)_3$	956	-93,12	-8,90
$ZrCl_4$	475	-89	-6,07

[a] $[\alpha]^D=\alpha/cl$; [b] Molar rotation = $[\alpha]^D*M_n$; commercial PLA

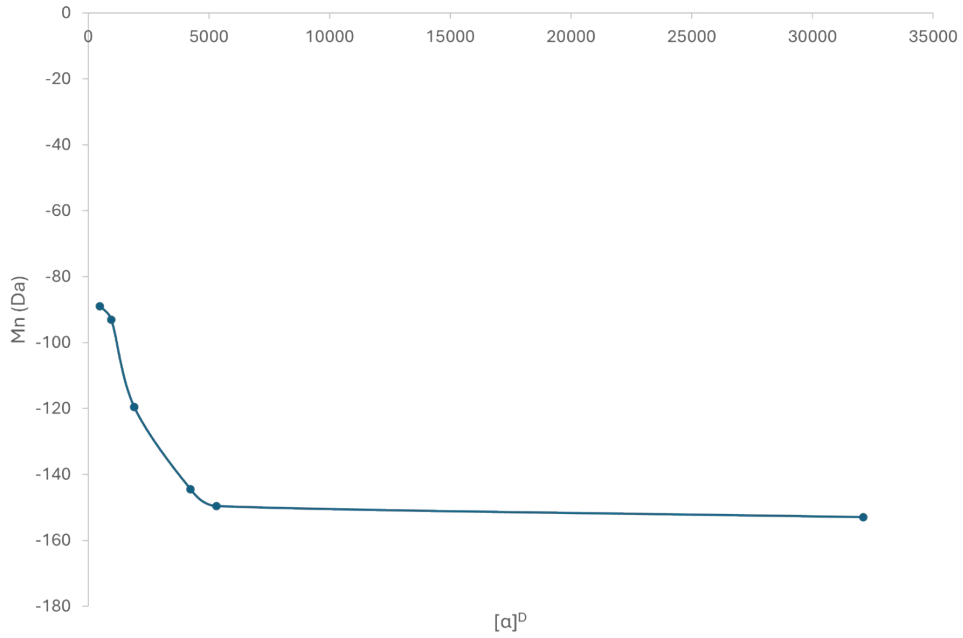

Figure S42. The variation of specific rotation with molecular weight. It shows that as the molecular weight (or degree of polymerization) increases the specific rotation varies linearly, after reaching the saturation the molecular weight variation is very small. In case of molar rotation, the linearity is applicable for all molecular weights.

S9. Reaction Temperature Profile

For **Entry 8, Table 1** a detailed study of the reaction temperature profile was carried out. The temperature was monitored at different heights and at various time intervals, as reported in the Table S8.

Table S8. Reaction Temperature Profile *vs* time *vs* distance

Temperature (°C)	Distance (cm)	Time (minute)
35	13	5
75	13	20
82	13	30
88	13	60
90	13	90
100	11,5	120
105	11,5	140
105	11,5	150
115	9	210
115	9	240
115	9	300
115	9	360

The lamp was initially positioned 13 cm from the reaction crucible; after 2 hours, the distance was reduced to 11.5 cm, and subsequently to 9 cm after 3 hours and 30 minutes. With the progressive approach of the lamp to the crucible and over time, the temperature showed a steady increase, reaching a maximum value of 115 °C.

As shown in the Figure S43, the temperature trend as a function of time is directly proportional, while the distance between the lamp and the crucible decreases over time and is therefore inversely proportional to the temperature.

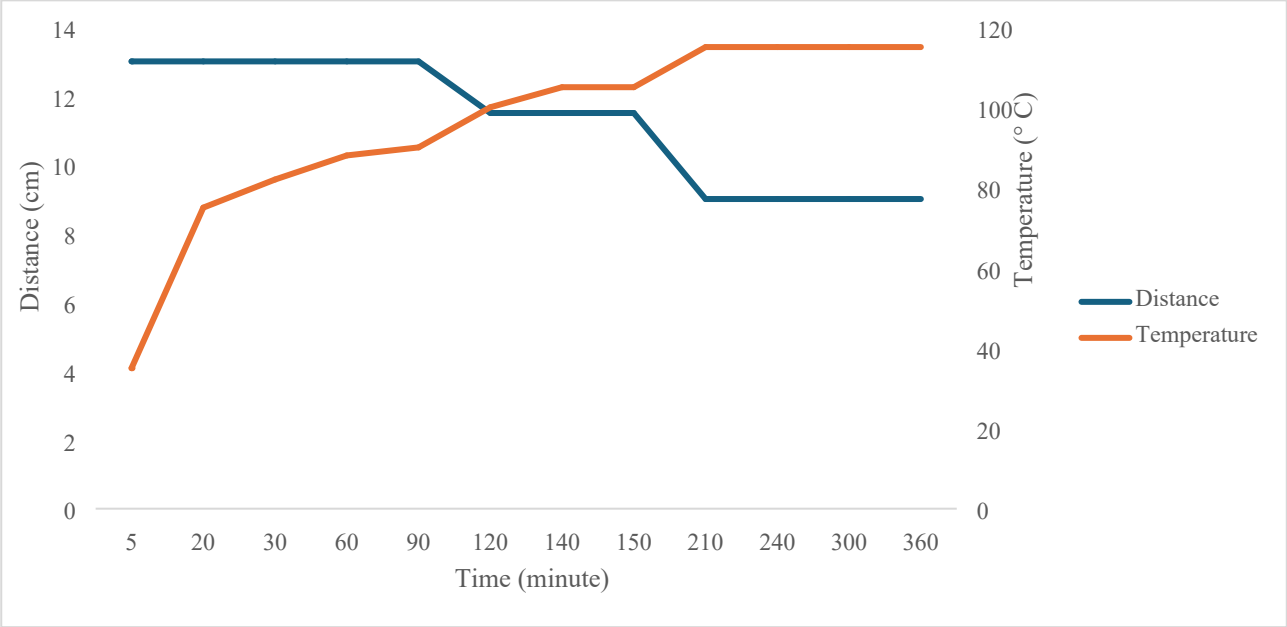

Figure S43. Temperature profile

S10. Catalyst recovery and recycle

The reaction (**Entry 4, Table 8**) was chosen to study the possibility of recovering and recycling $Sc(TfO)_3$. After the reaction, the solid was washed with demineralized water (100 ml), in which the catalyst is soluble, and sonicated for 30 minutes. The solid was then filtered through a Millipore glass funnel (0.1 µm pore size). The recovered water was evaporated and the solid residue obtained was dried for 1 hour at 100 °C and reused in the next reaction. The recovered catalyst was analyzed by (^{19}F-NMR, Figure S44 a and b) and reused (Figure S45).

a) **b)**

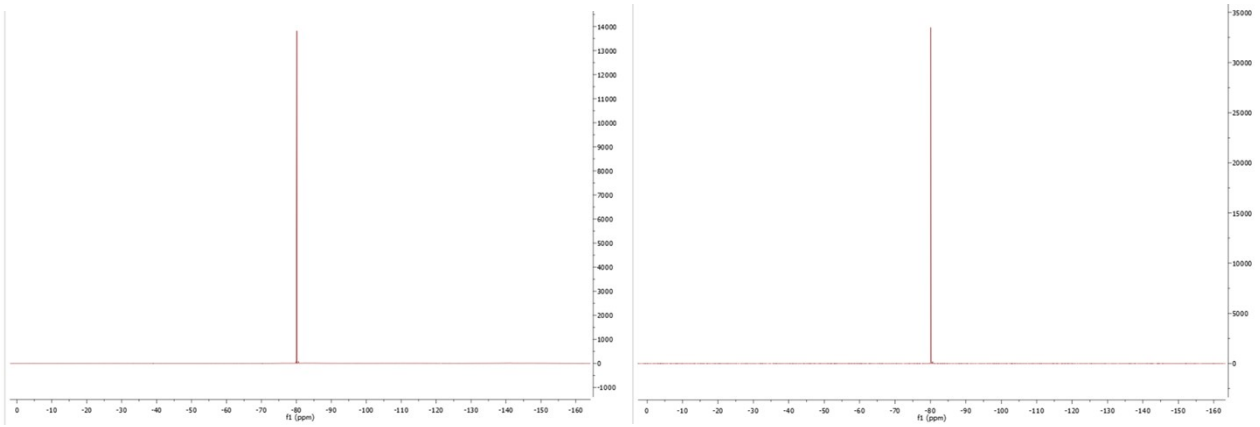

Figure S44: ^{19}FNMR (470 MHz, CD_3OD) spectrum of a) commercial $Sc(OTf)_3$ and b) recovery $Sc(OTf)_3$.

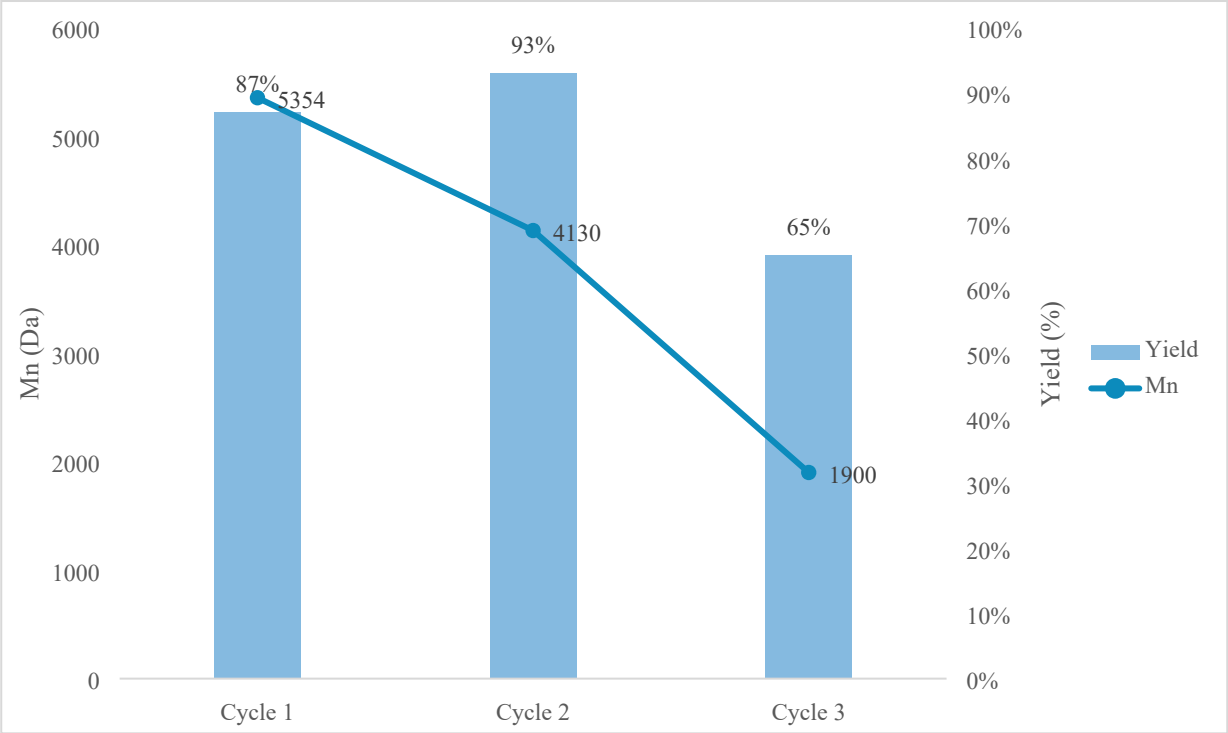

Figure S45: Reaction yields obtained in three consecutive cycles of catalyst recovery and reuse. For each cycle the corresponding molecular weights of the product are reported.

References

1. Lotz, B. Crystal Polymorphism and Morphology of Polylactides. In: Di Lorenzo, M., Androsch, R. (eds) Synthesis, Structure and Properties of Poly(lactic acid). Advances in Polymer Science, vol 279 (Springer, Cham 2017) (2017). https://doi.org/10.1007/12_2016_15
2. De Santis, P., & Kovacs, A. Molecular conformation of poly (S-lactic acid). *Biopolymers: Original Research on Biomolecules*, **6**, 299-306 (1968) https://doi.org/10.1002/bip.1968.360060305
3. Zhang, J. et al. Crystal modifications and thermal behavior of poly (L-lactic acid) revealed by infrared spectroscopy. *Macromolecules*, **38**, 8012-8021 (2005) https://doi.org/10.1021/ma051232r
4. Cartier, L. et al. Epitaxial crystallization and crystalline polymorphism of polylactides. *Polymer*, **41**, 8909-8919 (2000) https://doi.org/10.1016/S0032-3861(00)00234-2
5. Murthy, N. S. et al. Structure of the amorphous phase in crystallizable polymers: poly (ethylene terephthalate). *Macromolecules*, **24**, 1185-1189 (1991)
6. Stoclet, G. et al. Strain-induced molecular ordering in polylactide upon uniaxial stretching. *Macromolecules*, **43**, 1488-1498 (2010) https://doi.org/10.1021/ma9024366
7. Bao, Q., et al. Synthesis of polylactic acid oligomers for broad-spectrum antimicrobials. Polymers, 14(20), 4399 (2022) https://doi.org/10.3390/polym14204399